Diplomarbeit in Physik
angefertigt im
Helmholtz - Institut für Strahlen- und Kernphysik

Implantation studies of ^{111}In in group-III nitride ternary semiconductors

vorgelegt der
Mathematisch-Naturwissenschaftlichen Fakultät
der
Rheinischen Friedrich-Wilhelms-Universität Bonn

von
Sahar Hamidi

Bonn, November 10, 2010

Diplomarbeit in Physik
angefertigt im
Helmholtz - Institut für Strahlen- und Kernphysik

Implantation studies of ^{111}In in group-III nitride ternary semiconductors

vorgelegt der
Mathematisch-Naturwissenschaftlichen Fakultät
der
Rheinischen Friedrich-Wilhelms-Universität Bonn

von
Sahar Hamidi

Bonn, November 10, 2010

Anfertigung mit der Genehmigung
der Mathematisch-Naturwissenschaftlichen Fakultät
der Rheinischen Friedrich-Wilhelms-Universität Bonn

Referent: Privatdozent Dr. Reiner Vianden

Koreferent: Prof. Dr. K.-T. Brinkmann

I hereby certify that the work presented here was accomplished by myself and without the use of illegitimate means or support, and that no sources and tools were used other than those cited.

Bonn, den November 10, 2010

Contents

1. Introduction

The potential of group-III nitrides and their alloys for applications in optoelectronics and high-speed devices has attracted a great deal of interest. AlN, GaN and InN have direct band gaps with corresponding light emission ranging from visible to ultraviolet light. Their alloys have therefore direct band gaps that can be tuned to any favorable value in this range by varying the alloy composition. This offers many new possibilities for device engineering.
Moreover, the stability of these nitrides at high temperatures and a good thermal conductivity, make them a good choice for high frequency electronics.

Among these three ternary nitrides, $Al_xGa_{1-x}N$ has been subject of many interest due to its vast applications in semiconductor lasers, LEDs and in AlGaN/GaN high electron mobility transistors (HEMTs). Interesting results of measurements on AlN and GaN binary alloys suggest to study the lattice properties of this ternary compound, depending on the Al/Ga concentration.

For this purpose, AlN-content dependence measurements are performed in this work. By using different AlN-concentrations from 4% to 77%, the alterations of the lattice are studied and compared with previous results corresponding to AlN and GaN compounds ([SCH07]) as well as the measurements done by implanting ^{181}Hf ([GLV09]).

The temperature dependent band gap of this alloy is a good motive to study its lattice properties at different temperatures. The observation of temperature dependent defect densities is also of interest as it affects the operation of the AlGaN-based devices at high temperatures. The temperature dependence measurements are performed for three different AlN-concentrations: 19%, 55% and 77% so that the results can be compared with prior studies on the binary alloys AlN and GaN.

On the other hand, fundamental properties of $In_xAl_{1-x}N$ alloy are still not well studied. The lack of knowledge about this alloy is due to the difficulty of obtaining this alloy at a good quality. InAlN/GaN has the potential of being a novel alternative to AlGaN/GaN heterostructures. It can be lattice-matched to GaN with InN-concentration of about 17% and by increasing the stability of the heterojunction can provide a wider operation range of electric devices. Subsequently, the behavior of this specific compound in high temperatures is of experimental interest in the current work.

The Perturbed Angular Correlation (PAC) method, provides an insight into these

properties by insertion of radioisotope probes into the crystal lattice. By ion-implanting the ^{111}In radioisotope probe into $Al_xGa_{1-x}N$ and $In_xAl_{1-x}N$ samples, we can take advantage of the fact that the probes can substitute Al, Ga or In atoms in the sample.

Previous studies on AlN and GaN involving the PAC-probe ^{111}In revealed a reversible temperature behavior regarding the local structure surrounding the probes. In measurements at high temperature, all the probes are found on regular lattice sites and the lattice seems to be recovered. However, going back to lower temperatures, a large fraction of probes can again be found on disordered lattice sites. This reversibility was another subject of study in this work.

2. Group-III nitride semiconductors

Three different crystal structures are common for the group-III nitride crystals: wurtzite, zincblende and rocksalt structure. The thermodynamically stable and energetically favorable structure of these nitrides is wurtzite structure. The ternary alloys used in the present work, are of this kind.

This structure is made of two interpenetrated Hexagonal Close Packed (HPC) sublattices, each with one type of atoms, with an offset along $\hat{c}$-axis (fig. 2.1). In the ideal wurtzite structure, the offset $b = 3/8c$. In real crystals, this is parameterized using the u-parameter defined as $u = b/c$ and may deviate from its ideal value.

	AlN	GaN	InN
Band gap [eV]	6.20	3.44	0.9
Lattice constant a [Å]	3.112	3.189	3.533
Lattice constant c [Å]	4.982	5.185	5.693
u parameter	0.382	0.377	0.379
Density[g cm^{-3}]	3.23	6.15	6.81
Melting point [K]	3273	2773	1373
Thermal expansion $\frac{\Delta a}{a}$[K^{-1}]	4.2×10^{-6}	5.6×10^{-6}	3.8×10^{-6}
Thermal expansion $\frac{\Delta c}{c}$[K^{-1}]	5.3×10^{-6}	$3,2 \times 10^{-6}$	2.9×10^{-6}

Table 2.1: *Crystal parameters and properties of group-III nitrides at 300 K [MOR99][WEI96][IOFFE]*

Each atom is coordinated by four atoms of the other type forming a tetrahedron. The wurtzite structure has the stacking sequence of the (0001) planes as $ABAB$ in $\hat{c}$-axis direction. The different bonding length along $\hat{c}$-axis, caused an asymmetric charge distribution which leads to an intrinsic electric field gradient in $\langle 0001 \rangle$ direction in the crystal lattice. Tab. 2.1 shows the crystal parameters as well as the properties of AlN, GaN and InN.

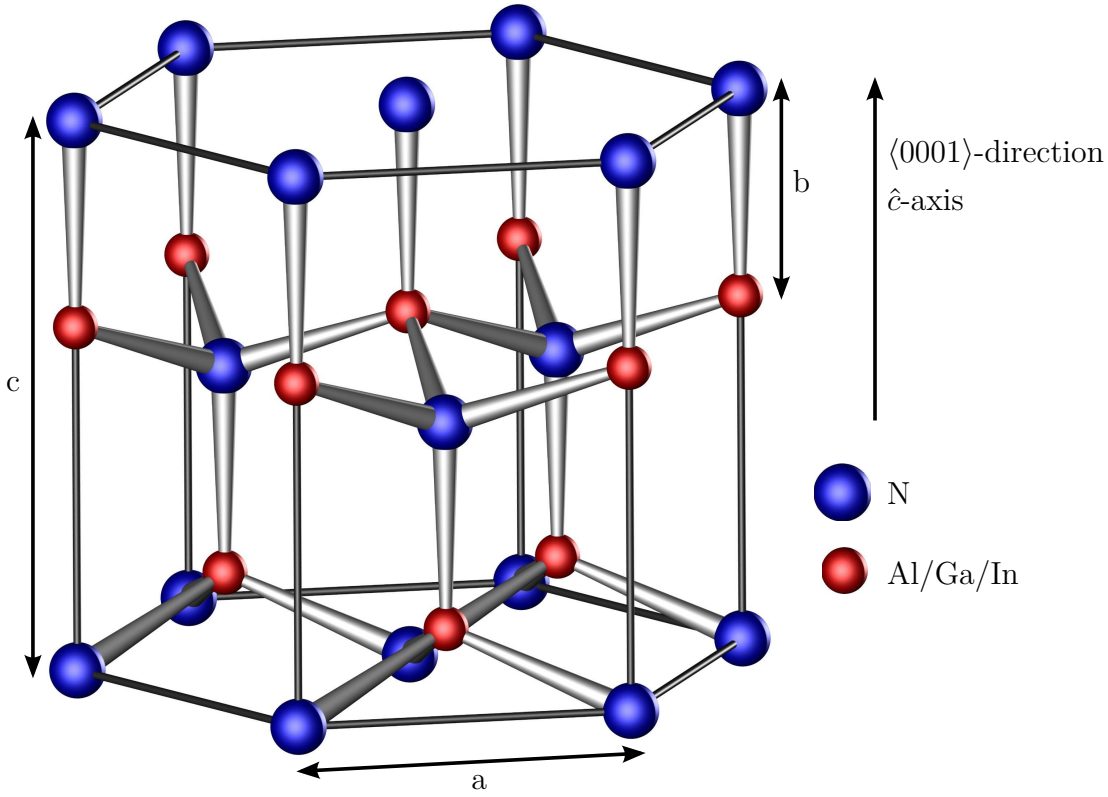

Figure 2.1: *The ideal wurtzite structure of the group-III nitride semiconductors [ARE]. In the ternary alloys AlInN and AlGaN, the red atoms are substituted by Al and In/Ga atoms. The different N bonding length in* ⟨0001⟩ *direction causes a field gradient in this direction.*

The properties of group-III nitride ternary alloys depend on the alloy composition. In spite of extensive studies on the properties of these alloys, such as energy band gap and effective electrons and holes masses, the obtained results are still not precise.

In general, the band gap of a ternary alloy can be expressed in a parabolic approximation:

$$E_{gap}^{AB}(x) = xE_{gap}^{A} + (1-x)E_{gap}^{B} - bx(1-x) \tag{2.1}$$

where $E_{gap}^{AB}(x)$ is the band gap of an A_xB_{1-x} alloy, E_{gap}^{A} and E_{gap}^{B} are the band gaps of the constituents and x denotes the A's molar fraction. b is called bowing parameter and characterizes the nonlinear dependence of the fundamental band gap on the alloy composition.

In the case of an $Al_xGa_{1-x}N$ alloy, A and B are corresponding to AlN and GaN, respectively. The reported experimental values vary from -0.8 eV to 2.6 eV related to the growth temperature of the AlGaN layers [LEE99] [MHP].

Despite the importance of $In_xAl_{1-x}N$ to provide a lattice-matched barrier to GaN, its properties have not been studied vastly. The energy gap of this alloy is also described by eq. (2.1). The experimental results for the b parameter, show a ranging from 4.76 eV for $x = 0.25$ to 2.20 eV for $x = 0.75$ [DBR03]. Nevertheless, studies of Iliopoulos et. al. denote that the bowing parameter of $In_xAl_{1-x}N$ is strongly dependent on composition [IAG08].

3. Measuring Method

3.1 Perturbed angular correlation

In this chapter the aspects of **P**erturbed γ-γ-**A**ngular **C**orrelation (PAC) will be discussed. This technique can be used to derive the internal electromagnetic fields in solids by using nuclei with known magnetic dipole and electric quadrupole moments. In sec. 3.1.1 the principles of unperturbed angular correlation will be reviewed. Then in sec. 3.1.2 the perturbation due to electric field gradient (EFG) in the intermediate state of the radioactive probe will be discussed.

Afterwards, ^{111}In decay to ^{111}Cd is reviewed in sec. 3.2, as it is one of the most often used probe nuclei in PAC and used in measurements of this work. Finally, in sec. 3.3 the experimental setup and data reduction is explained.

3.1.1 Unperturbed γ-γ-angular correlation

The emission of the first γ-ray is isotropic; although, its detection in a fixed direction, $\mathbf{k_1}$, causes the probability of emission of the succeeding γ-ray to be anisotropic. In other words, through successive emission of two γ-quanta, the direction of second radiation has a certain angular correlation with the first one. The initial state $|I_i, M_i\rangle$ decays via emission of γ_1 into the intermediate state $|I, M\rangle$ which itself decays into the final state $|I_f, M_f\rangle$ (fig. 3.1). The aim is to find the angular correlation function $W(\mathbf{k_1}, \mathbf{k_2})$, which is defined as the probability that a nucleus emits γ_1 and γ_2 in directions $\mathbf{k_1}$ and $\mathbf{k_2}$ respectively, through the cascade $|I_i, M_i\rangle \rightarrow |I, M\rangle \rightarrow |I_f, M_f\rangle$. This is shown briefly in the following and the comprehensive explanation can be found in [FS65]. The angular correlation can

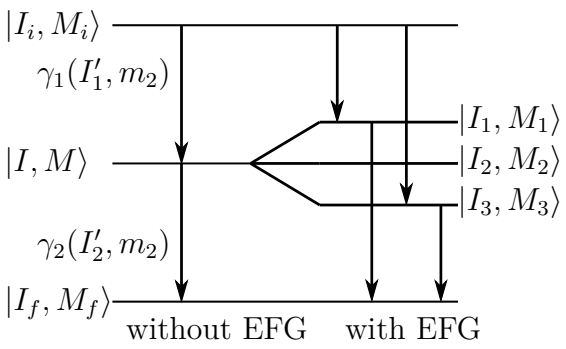

Figure 3.1: *An example for 0-1-0 γ-γ-cascade in the absence and presence of electric field gradient [SW92].*

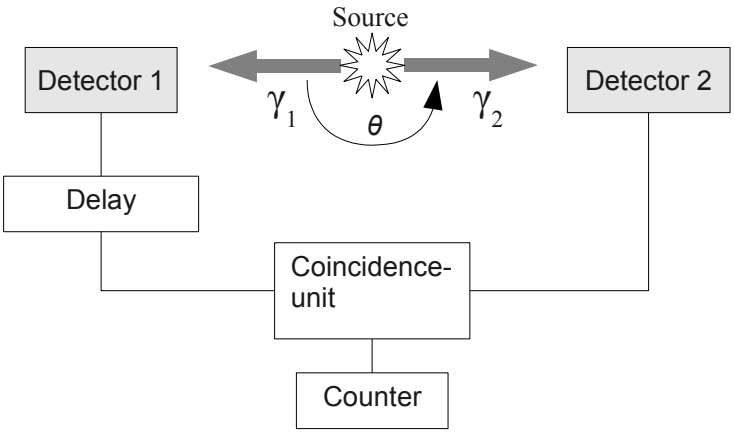

Figure 3.2: *Principle of γ-γ-angular correlation. Detecting γ_1 is the start signal of the life time measurement and detecting γ_2 is the stop signal.*

be written as

$$W(\mathbf{k_1}, \mathbf{k_2}) = \sum_{M_i, M_f, \sigma_1, \sigma_2} \left| \sum_{M} \langle M_f | H_2 | M \rangle \langle M | H_1 | M_i \rangle \right|^2 \tag{3.1}$$

Here H_i is the interaction operator for emission of γ_1 into direction $\mathbf{k_1}$ with polarization σ_i [SW92]. Calculating the matrix elements leads to the equation:

$$W(\mathbf{k_1}, \mathbf{k_2}) = W(\theta) = \sum_{k\,even}^{k_{max}} A_k(1) A_k(2) P_k(\cos\theta) \tag{3.2}$$

where k is the summation index and $0 \leq k \leq \mathrm{Min}\{2I, L_1 + L_1', L_2 + L_2'\}$. Due to conservation of parity, the k have to be even. The coefficients $A_k(1)$ and $A_k(2)$ depend only on the first and second transition respectively. $P_k(cos\theta)$ is the Legendre polynomial in order of θ, the angle between $\mathbf{k_1}$ and $\mathbf{k_2}$, and I is the nuclear spin of the intermediate state. L_1,L_2,L_1',L_2' are multipolarities of the transitions. Using ^{111}In as probe nuclei, the nuclear spin of the intermediate state is $I = \frac{5}{2}$, therefore $L_1 = 1$, $L_2 = 2$ and $k_{max} = 4$.

3.1.2 Perturbed γ-γ-angular correlation

The radioactive nuclei are implanted in the lattice and on the lattice site, the probe experience magnetic or electric hyperfine interaction with extranuclear electromagnetic fields. The hyperfine interaction lifts the degeneracy of the intermediate state and causes the second γ-ray to be emitted after repopulation or phase change of magnetic substates of this state. Considering $|M_a\rangle$ as an initially

populated sublevel, its time evolution can be described as:

$$|M_a\rangle \rightarrow \Lambda(t)|M_a\rangle = \sum_{M_b} |M_b\rangle\langle M_b|\Lambda(t)|M_a\rangle \tag{3.3}$$

where $\Lambda(t)$ is the time evolution operator. Replacing $|M\rangle$ by $\Lambda(t)|M\rangle$, a time dependent perturbation is introduced into the angular correlation and the time evolution of sublevel population with the time between emission of both γ-rays is considered. This leads to:

$$W(\mathbf{k_1}, \mathbf{k_2}, t) = \sum_{M_i, M_f, \sigma_1, \sigma_2} \left| \sum_{M_a} \langle M_f|H_2\Lambda(t)|M_a\rangle\langle M_a|H_1|M_i\rangle \right|^2 \tag{3.4}$$

Calculation leads to following form for the time-dependent γ-γ-angular correlation:

$$W(\mathbf{k_1}, \mathbf{k_2}, t) = \sum_{k_1, k_2, N_1, N_2} A_k(1)\ A_k(2)\ G^{N_1 N_2}_{k_1 k_2}(t) \frac{Y^{N_1^*}_{k_1}(\theta_1, \phi_1)\ Y^{N_2}_{k_2}(\theta_2, \phi_2)}{\sqrt{(2k_1+1)\,(2k_2+1)}} \tag{3.5}$$

Here $G^{N_1 N_2}_{k_1 k_2}(t)$ is called perturbation function and describes the effect of external perturbation on the probe. It has the form:

$$\begin{aligned} G^{N_1 N_2}_{k_1 k_2}(t) \;=\; & \sum_{M_i, M_j} (-1)^{2I+M_i+M_j} \sqrt{(2k_1+1)\,(2k_2+1)} \\ & \cdot \begin{pmatrix} I & I & k_1 \\ M_i' & -M_i & N_1 \end{pmatrix} \begin{pmatrix} I & I & k_2 \\ M_j' & -M_j & N_2 \end{pmatrix} \langle M_j|\Lambda(t)|M_i\rangle\langle M_j'|\Lambda(t)|M_i'\rangle^* \end{aligned} \tag{3.6}$$

where N_i are restricted to $|N_i| \leq k_i$ and k_i also have the same limitation as the unperturbed case; i.e. k_i are even and $0 \leq k_i \leq \mathrm{Min}\{2I, L_1 + L_1', L_2 + L_2'\}$. The $Y^{N_i}_{k_i}$ are spherical harmonics, the angles θ_i and ϕ_i are defined in fig. 3.3.

By restricting attention to axially symmetric perturbations, e.g. magnetic interaction and axially symmetric electric quadrupole interactions, the Hamiltonian in eq. (3.4) is always diagonal and analytic calculation of eqs. (3.5) and (3.7) is possible. The perturbation function which causes a time-dependent oscillation of the angular correlation can be written as:

$$G_{k_1 k_2}(t) = \exp(-i\omega t) \tag{3.7}$$

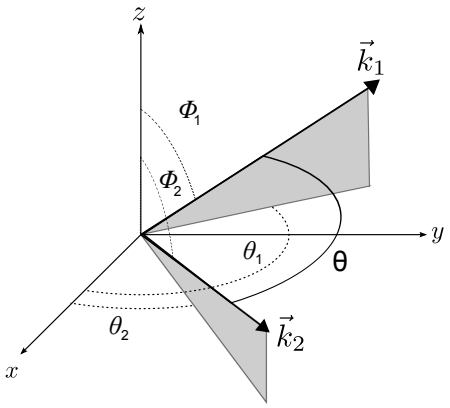

Figure 3.3: *Coordinate system for the γ-γ-angular correlation used in eq. 3.5.* $\mathbf{k_1}$ *and* $\mathbf{k_2}$ *show the wave vectors of* γ_1 *and* γ_2 *which are detected by first and second detector respectively.*

Here ΔE shows splitting and shifting from the unperturbed intermediate level and ω is called the transition rate between individual M-substates.

Electric interactions which are the subject of interest, are caused by coupling of EFGs at the probe nucleus site, to quadrupole moment, Q, of the nucleus. EFGs that are strong enough to be measured by PAC are found in non-cubic crystal structures or non-complete electron shells. EFG is defined as the second derivative of the electric potential, Φ, at the nuclear site:

$$V_{ij} = \frac{\partial^2 \Phi}{\partial x_i \partial x_j} \qquad \text{for } i,j = 1,2,3 \tag{3.8}$$

The nine component of this traceless tensor can be decreased to three diagonal elements by choosing a suitable coordinate system, in which $|V_{zz}| \geq |V_{yy}| \geq |V_{xx}|$. To fulfill the Poisson equation, only two independent elements are needed to fully describe the EFG. It is conventional to choose the largest component, V_{zz} and the asymmetry parameter. The latter is defined as:

$$\eta := \frac{V_{xx} - V_{yy}}{V_{zz}} \qquad \text{with } \; 0 \leq \eta \leq 1 \tag{3.9}$$

The assymmetry parameter η contains information about the deviation from the axial symmetric EFG, ($V_{xx} = V_{yy}$), and therefore of the lattice structure. In the case of axially symmetric field ($\eta = 0$) the interaction Hamiltonian is diagonal and the corresponding eigenvalues can be written as:

$$E_m = \frac{eQV_{zz}}{4I(2I-1)} \left[3m^2 - I(I+1)\right] \tag{3.10}$$

where Q is the nuclear electric quadrupole moment of the intermediate level. The energy differences between the substates are:

$$\Delta E = E_m - E_{m'} = \frac{3eQV_{zz}}{4I(2I-1)} \left|m^2 - m'^2\right| \tag{3.11}$$

To describe the interaction, the quadrupole frequency is defined as the frequency which is independent of the magnetic quantum number of the states:

$$\omega_Q := \frac{eQV_{zz}}{4I(2I-1)\hbar} \tag{3.12}$$

Consequently, the energy difference in eq. (3.11) can be written as:

$$\Delta E = 3 \left|m^2 - m'^2\right| \hbar\omega_Q \tag{3.13}$$

The smallest observable transition frequency between different sublevels is related to the quadrupole frequency as:

$$\begin{aligned} \omega_0 &= \frac{3eQV_{zz}}{4I(2I-1)\hbar} = 3\omega_Q \qquad \text{for half integer spin,} \\ \omega_0 &= \frac{6eQV_{zz}}{4I(2I-1)\hbar} = 6\omega_Q \qquad \text{for integer spin.} \end{aligned} \tag{3.14}$$

In the case of axially symmetric electric field gradients, the higher transition frequencies, ω_n, are integer multiples of the lowest frequency: $\omega_n = n\omega_0$. For ^{111}In with spin $I = 5/2$, the transition frequencies (fig. 3.4) are:

$$\begin{aligned} \omega_1 &= 1\omega_0 = 6\omega_Q \\ \omega_2 &= 2\omega_0 = 12\omega_Q \\ \omega_3 &= 3\omega_0 = 18\omega_Q \end{aligned}$$

The interaction strength at the site of the probe nucleus is expressed by quadrupole interaction frequency (QIF), which is independent of the nuclear spin I:

$$\nu_Q = \frac{eQV_{zz}}{h}. \tag{3.15}$$

With these assumptions, the general form of the correlation function in eq. (3.5) can be written as:

$$W(\theta_1, \phi_1, \theta_2, \phi_2, t) = 1 + A_{22} G^{NN}_{k_1 k_2}(t) \tag{3.16}$$

where

$$G^{NN}_{k_1 k_2} = \sum_{n=0}^{3} s^{k_1 k_2}_{nN} \cos(\omega_n t). \tag{3.17}$$

Apparently, the perturbation function $G^{NN}_{k_1 k_2}$ is a superposition of cosine functions of transition frequencies with weight $s^{k_1 k_2}_{nN}$ which are carrying all the information about geometry of the arrangement. That means they depend on asymmetry parameter, η, the angle between $\mathbf{k}_1$ and $\mathbf{k}_2$, as well as orientation of the EFG and detectors relative to the crystal lattice. The solutions for specific cases can be found in [BEZ98] and [WEG85].

3.2 ^{111}In as probe nucleus

A radioactive source that is used in PAC technique must have an isomeric level with a lifetime in the range of few nanoseconds to some microseconds. The lower limit is determined by the time resolution of the experimental setup. The upper restriction for life time is due to optimization of signal-to-noise ratio which decreases as $1/\tau_N$. On the other hand, the quadrupole moment of the intermediate level has to be large enough ($Q \geq 0.1$ barn) so that the corresponding ω_Q can be measured during the interaction [SW92].

These requirements are well fulfilled for ^{111}In. It decays to ^{111}Cd by electron capture (EC) and has a half life of 2.83 days (Fig. 3.2). The intermediate level of the cascade with spin 5/2, has a half life of 85 ns and a quadrupole moment

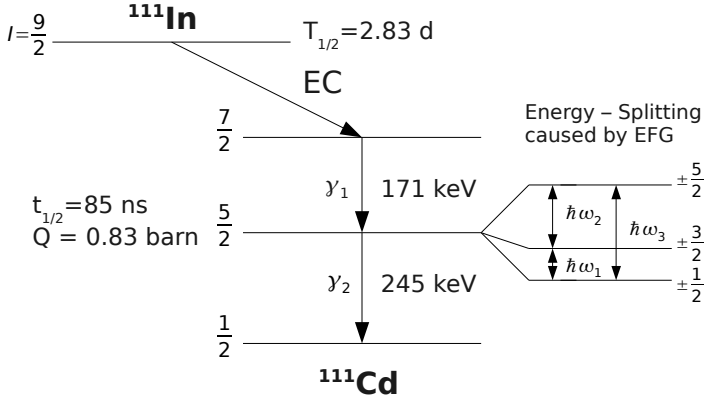

Figure 3.4: *The decay scheme of ^{111}In. It decays to the excited state of ^{111}Cd by electron capture, then through a γ-γ-cascade to its ground state. The degeneracy of the isomeric intermediate states are strongly magnified on the right.*

of 0.83 barn. The first and the second γ-emissions have 171 keV and 245 keV respectively. The detection of γ_1 is used as start signal of the measurement and γ_2 as stop signal.

A further advantage of using ^{111}In as probe nucleus in PAC measurement of AlInN and AlGaN, arises by the fact that it belongs to third group of elements and has the same electronic structure as Al and Ga. ^{111}In atoms can substitute Al and Ga atoms in the host lattice making small perturbation caused by different atom radii.

3.3 Experimental techniques

3.3.1 PAC-spectrometer

In the perturbed angular correlation method the angular correlation is measured as a function of the time between detection of γ_1 and γ_2. This time is measured by the coincident detection of the subsequently emited γ-quanta, the start and stop signals in the measurement.

Without any interaction with extranuclear fields, the probability that the second γ-ray is detected at time t after the first one, decays exponentially weighted by time-independent angular correlation $W(\theta)$ for a specific detector angle. In the presence of a field gradient at the site of the decaying nuclei, the decay curve is modified by replacing the time-dependent angular correlation as the weight of the

decay. In fig. 3.5 a simplified pattern of these spectra is shown. The exponential decay is removed from the spectra (fig. 3.5 down) as it is explained in sec. 3.3.2, to extract the perturbation function.

Measurements of the current work are done in four-detector-spectrometer in which BaF_2 had been used as scintillator material in detectors.Operation of the spectrometer is based on the fast-slow delayed coincidence technique and is described in literature, e.g.[LOR02].

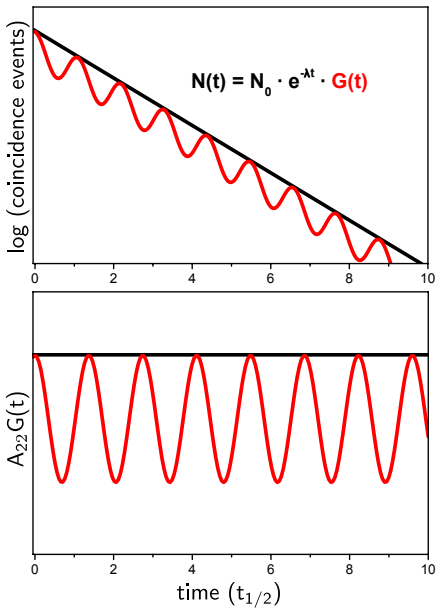

Figure 3.5: *In the upper graph the life time curve of the nuclei is shown in black while the green curve is the modulated lifetime in the presence of a field gradient at the probe's site. In the lower graph, the perturbation function is obtained by removing the exponential decay.*

3.3.2 Data analysis

To extract the internal fields' information from the measured time coincidence spectra, it should be comparable to the theoretical correlation functions. Hence, exponential decay, detector efficiencies and factors have to be removed from the spectra. The data reduction methods are studied in detail by Arends et al. [ARE80].

First, the coincidence count rate of detector i and j is assumed to be a function of θ, the angle between two detectors, and t, the time between start and stop signals. This can be written as

$$N_{ij}(\theta,t) = N_0\epsilon_i\epsilon_j\Omega_i\Omega_j \cdot \exp\left(-\frac{t}{\tau_n}\right) \cdot W(\theta,t) + U \tag{3.18}$$

where N_0 is the activity of the source at time zero and τ_n is life time of the intermediate state. ϵ_i and ϵ_j are detector efficiencies, Ω_i and Ω_j are the solid angles covered by the detectors and U is the background of random coincidences. These coincidences are caused by detection of γ_1 and γ_2 from different nuclei and are removed form the spectra. The random count rate between two detectors is

$$N_{ij}^R = \epsilon_1\epsilon_2\Omega_1\Omega_2N_0^2 \tag{3.19}$$

[SW92]. In the next step, the background data is removed as well as exponential decay. Additionally, angular correlation measured for the randomly oriented and axially symmetric EFGs, is substituted in eq. (3.18), as below:

$$W(\theta,t) \approx 1 + A_{22} \cdot G_{22}(t) \cdot P_2(\cos\theta) \tag{3.20}$$

Recording twelve spectra from different combinations of the four detectors, the time-dependent ratio function, $R(t)$, can be defined as below,

$$R(t) = 2 \cdot \frac{N(180°, t) - N(90°, t)}{N(180°, t) + 2 \cdot N(90°, t)} \tag{3.21}$$

Since detector efficiencies and solid angles appear both in nominator and denominator, $R(t)$ is independent of these factors. The program ShowFit, written by [RUS01] is used to calculate the $R(t)$-function. Assuming $|A_{44}| \ll 1$, the ratio function can be simplified as:

$$R(t) \approx A_{22} \cdot G_{22}(t) \tag{3.22}$$

Hence, from measured $R(t)$-functions, the perturbation function $G_{22}(t)$ can be deduced. In general case, there exist more than one perturbation, caused by different environments in the lattice. Therefore, the measured perturbation function is a linear superposition of all the perturbations, $G_i(t)$, associating the interactions:

$$G(t) = \sum_i f_i G_i(t) \quad \text{and} \quad \sum_i f_i = 1 \tag{3.23}$$

where $G_i(t)$ is defined in eq. (3.7) and f_i is the fraction of the probes subjected to the perturbation $G_i(t)$.

Fitting the spectra is done by the Nightmare, written by [NÉD07], based on NNFit [BAR92]. The ratio function calculated by the Nightmare with the least square method, includes theses parameters:

QIF , ν_{Qi} [MHz], of a oscillation in the $R(t)$-spectra. ν_Qs describe the strength of different EFGs in the lattice.

fraction of the probes , f_i, [%], is the amplitude of the ith frequency and displays the fraction of the probes exposed to a particular EFG.

damping factor , δ_i [%], of an oscillation denotes the width the ith EFG distribution, demonstrating that the EFG is not single valued.

asymmetry parameter , η, shows the deviation from axial symmetric EFG

angle , θ, with respect to start detector, gives the direction of EFGs

To characterize different probe environments of the lattice, denoted as f_i s, they can be set as single-crystalline or polycrystalline in the Nightmare program. Setting a fraction as single-crystalline, a specific direction is assumed for the existing field gradient.

Nevertheless, to describe the multi-directional field gradient in the lattice, the studying fraction can be set as polycrystalline. Apparently, a polycrystalline fraction can be characterized as superposition of single-crystalline fractions in all the lattice directions.

4. Sample preparation

The samples studied in the present work are $In_xAl_{1-x}N$ and $Al_xGa_{1-x}N$ with different molar fractions of AlN. The former are obtained from Magdeburg University[1] are about 100 nm thick and grown on silicon substrates. The latter samples with 500 nm thickness are obtained from TDI[2] and grown on sapphire substrates. The nitride layers are grown so that the crystal's $\hat{c}$-axis is perpendicular to the surface.

The samples have to be implanted and tempered before the measurement; however, it is possible to measure a sample before tempering to observe the defects caused by implantation.

The sample size is limited to $5 \times 5\,\mathrm{mm}^2$ in the case of temperature dependent measurements due to the heating device's inner diameter (sec. 4.2).

4.1 Implantation

The implantation is done at the Bonn Isotope Separator. Since the In-metal has a high boiling point (2207 °C), $^{111}InCl_3$ solution[3] which evaporates at 418 °C is used [UNB98].

At the Bonn Isotope Separator, the samples can be implanted with energies up to 160 keV and under different angles. Through the solution's evaporation, the In is ionized and accelerated in an electric field. Afterwards, ions with mass 111 u can be selected by passing through a magnetic field. At last, the ^{111}In ions are accelerated with the appropriate energy and implanted in the sample. It should be considered that a relatively small part of stable decay products ^{111}Cd are also implanted. Therefore, the fluence of radioactive implanted ^{111}In, is smaller than the overall implanted particle fluence (about $5 \times 10^{11}\,\frac{1}{\mathrm{cm}^2}$ to $5 \times 10^{12}\,\frac{1}{\mathrm{cm}^2}$).

[1] Otto-von-Guerricke-Universität Magdeburg, Postfach 4120, D-39016 Magdeburg

[2] Technologies and Devices International Inc., 12214 Plum Orchard Drive, Silver Spring, MD 20904, USA

[3] Obtained from Covidien Deutschland GmbH, Gewerbepark 1, Neustadt 93333, Donau

The optimum implantation energy is estimated with the program SRIM 2008 [BH80], a Monte Carlo simulation program, that calculates the distribution of stopped ions in the target material (fig. 4.1). Moreover, according to [SCH07], an angle between 5° and 10° is appropriate for AlN to avoid channeling. In the current work, the $In_xAl_{1-x}N$ samples are implanted under 7° and the $Al_xGa_{1-x}N$ samples under 0°, where the samples are 500 nm thick and channeling cannot affect the measurements.

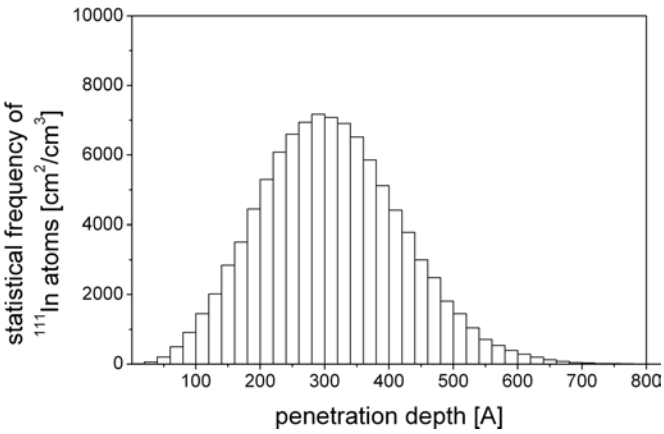

Figure 4.1: *SRIM simulation of implanting AlN with* ^{111}*In with an energy of* 60 keV*. The mean penetration depth is* 31.1 nm *with a standard deviation of* 11.0 nm*. The maximum penetration depth is below* 80 nm*.*

4.2 Annealing

The lattice is damaged during the implantation process, therefore the sample is tempered in a RTA-unit[4] [MAR90]. For this purpose, the sample is put between two graphite stripes, that are fixed between two electrodes of the RTA-unit. In order to control the sample's temperature, a thermocouple is fixed in the middle of the lower stripe, which is in contact with the sample. By adjusting the voltage, the temperature of the sample can be increased up to the desired value in a few seconds. The necessary annealing-temperature and -duration are known from previous studies [LOR02] and [KEI01].

$In_xAl_{1-x}N$ samples are tempered at different temperatures from 500 K to 1100 K for 120 s. The $Al_xGa_{1-x}N$ samples at 1223 K for 10 min.

To protect the sample from the out-diffusion of nitrogen, a so-called proximity cap, of the same material, is put on the sample's surface. In this way, the nitrogen's diffusion from sample at high temperatures is compensated by that of the proximity cap. For the same reason, the annealing is performed under nitrogen flow of 75 $\frac{\ell}{\mathrm{h}}$.

[4] Rapid Thermal Annealing

4.3 PAC-furnace

For the purpose of temperature dependent measurements, a heating unit is used which can be placed between the detectors. This unit is fabricated in a way, that can provide the measurement procedure between room temperature and 1200 °C[SR93].

The single crystalline sample is placed in a sample holder which will be set in a graphite heater. This heater is a graphite tube that is slitted from the bottom up to its cap. A thermocouple device is inserted inside the holder from top, as close as possible to the sample, to measure its temperature (fig. 4.2). The temperature control is realized by the PID control [STE07] adjusting voltage in an appropriate way.

In order to protect the detectors from the high temperature generated in the furnace, a liquid cooled temperature shielding is used. To avoid significant absorption of γ rays, the cooling liquid is pumped between two only 0.3 mm thick Al-tubes. More details about structure and performance of the PAC-furnace can be found in [ARE10] and [SR93].

Temperature dependent measurements can be done in the furnace either under nitrogen flow or in vacuum. In the present work, all measurements are performed in vacuum.

Figure 4.2: *Schematic construction of the PAC-furnace [ARE10]. The sample is fixed on a sample holder (white) which is placed in the graphite heater.*

5. Measurements of $Al_xGa_{1-x}N$

The 500 nm thick $Al_xGa_{1-x}N$ samples are implanted with ^{111}In with an energy of 60 keV under an angle of 0°.

Since AlN has a lower density than GaN, the former is taken into account to find an upper limit for the implantation depth using SRIM 2008 simulation. The results show the mean implantation depth of 31.1 nm and width of 11.0 nm (fig. 4.1). This is smaller than the thickness of the $Al_xGa_{1-x}N$ layer on the samples and channeling cannot affect the measurements. The specific sapphire EFG, observed by [SCH07], is not seen in the recorded PAC-spectra. Observing this field gradient indicates that the probe nuclei were implanted into the substrate.

All six $Al_xGa_{1-x}N$ samples are annealed in the RTA-unit at $T_A = 1223\,K$ for 10 min. This is done under nitrogen atmosphere, using proximity caps of the same samples. The sample treatment as well as the implantation angle and energy, is the same as the measurements done in the ISOLDE experiment, at CERN, so that the results can be comparable.

5.1 AlN-concentration measurements of $Al_xGa_{1-x}N$

To study the behavior of $Al_xGa_{1-x}N$ depending on AlN-concentration, x, the PAC-spectroscopy is performed for samples with 4%, 15%, 19%, 54%, 69% and 77% AlN-content. It's selected $R(t)$-spectra are shown in fig. 5.2, tab. 5.1 and fig. 5.1 display the results of the measurements' data analysis.

The spectra recorded from samples with 77%, 15% and 4% AlN-content, can be described using three parts; one polycrystalline fraction and two single crystalline ones. The single crystalline part with lower frequency, f_1, points out the probes at undisturbed substitutional Al or Ga sites, while the one with higher frequency ,f_2, denotes the probes subjected to a strong EFG which is typical for a point defect at the probe atom's vicinity. The high frequency of the polycrystalline part, f_3, implies EFGs in various directions, due to highly disordered environment.

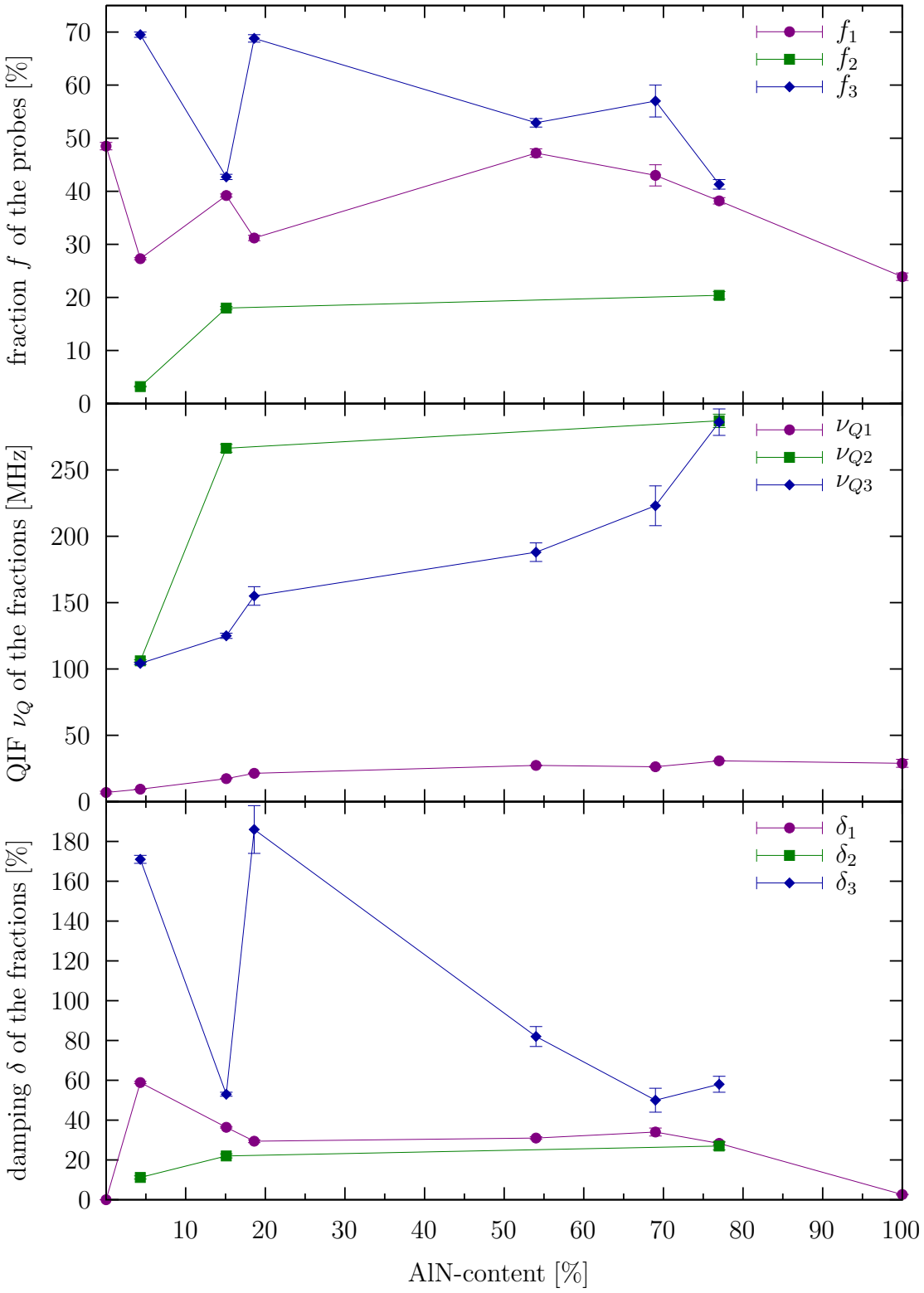
fraction f of the probes [%]
f_1
f_2
f_3
QIF ν_Q of the fractions [MHz]
ν_{Q1}
ν_{Q2}
ν_{Q3}
damping δ of the fractions [%]
δ_1
δ_2
δ_3
AlN-content [%]

Figure 5.1: *Results of PAC-measurements for the $Al_xGa_{1-x}N$ samples, tempered at $T_A = 1223\,\mathrm{K}$, depending on AlN-content.*
For the samples with the highest and lowest AlN-content, three fit components are needed: two single crystalline fractions, one with lower and one with higher frequency, as well as a polycrystalline fraction with high frequency. Though, the spectra from samples with intermediate AlN-content, are described by two components, a single crystalline and a polycrystalline fraction. f_1 shows the fraction of the probes on substitutional Al or Ga site, whereas f_2 and f_3 denote the fraction of the probes on the V_N sites. ν_{Q1}, which refers to the EFG caused by undisturbed lattice, increases with AlN-content in agreement with previous measurements of ^{181}Hf implanted $Al_xGa_{1-x}N$ [GLV09].

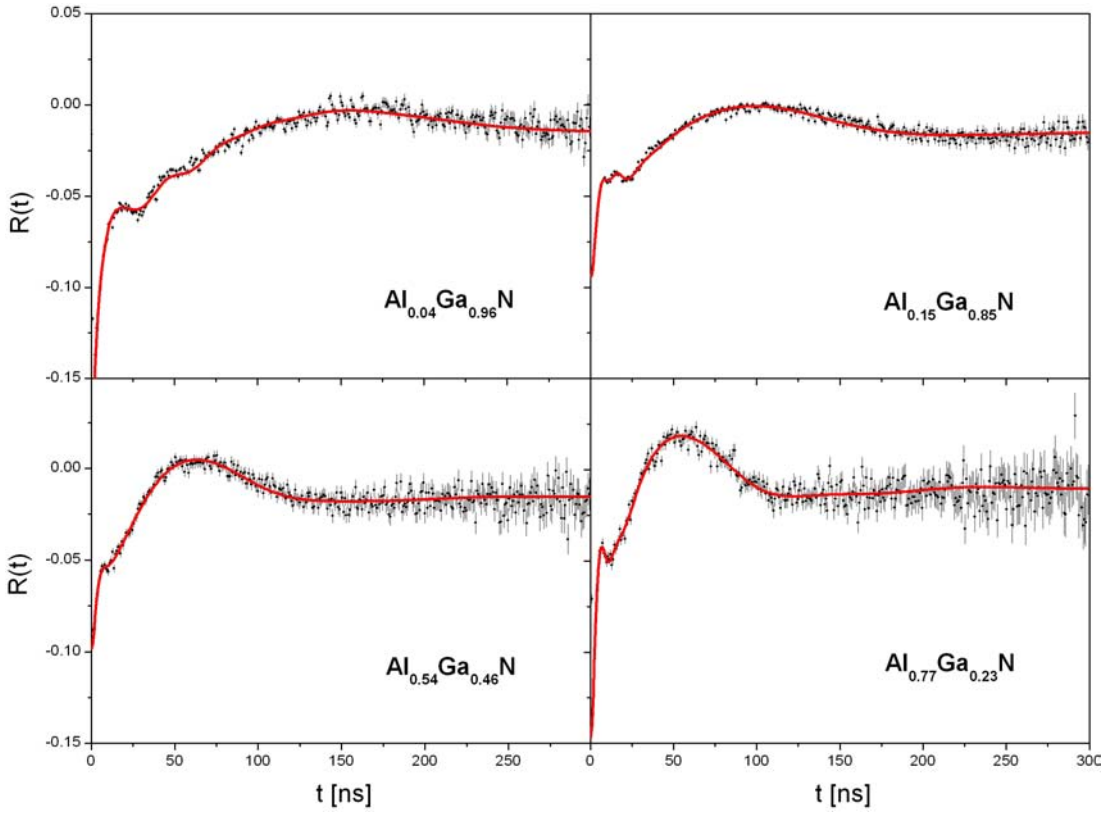

Figure 5.2: *PAC-spectroscopy of ^{111}In in $Al_xGa_{1-x}N$ at selected AlN-contents. The complete set of spectra can be found in fig. C.1.*

Al content x	0.04	0.19	0.54	0.77
f_1 [%]	27.3(2)	31.2(5)	47.2(8)	38.2(6)
ν_{Q1} [MHz]	9.42(4)	21.4(2)	27.3(4)	30.8(2)
δ_1 [%]	58.9(6)	29.4(7)	31.0(7)	28.3(8)
f_2 [%]	3.2(1)	–	–	20.4(7)
ν_{Q2} [MHz]	106.1(9)	–	–	287(5)
δ_2 [%]	11.2(8)	–	–	27(2)
f_3 [%]	69.5(5)	68.8(7)	52.9(8)	41.3(9)
ν_{Q3} [MHz]	104.2(8)	155(7)	188(7)	286(10)
δ_3 [%]	171(2)	186(12)	82(5)	58(4)

Table 5.1: *Results of some PAC-measurements for tempered $Al_xGa_{1-x}N$ samples ($T_A = 1223\,\mathrm{K}$) depending on the AlN-content. The first and second fractions are set as single crystalline part and third one shows the polycrystalline fraction of the probes' environment. The complete set of results is shown in tab. B.2*

The spectra corresponding to the samples with intermediate x-values (19%, 54% and 69% AlN-content) however, can be characterized using two components, a single crystalline one with low frequency describing the fraction of the probes on undisturbed lattice sites and a polycrystalline one with high frequency, illustrating multi-directional EFGs caused by point-defects.

In tab. 5.1 and fig. 5.1 the data analysis results of PAC-measurements are shown, as well as some results of AlN and GaN studies, done by [NIE09] and [SCH07].

f_1 rises from 27.3(2)% for $Al_{0.04}Ga_{0.96}N$ to 47.2(8)% for $Al_{0.54}Ga_{0.46}N$ and then declines nearly linearly to 38.2(6)% for $Al_{0.77}Ga_{0.23}N$. In between, two values related to GaN and $Al_{0.15}Ga_{0.85}N$ are notably higher than the adjacent values, describing a large fractions of the probes on the undisturbed lattice environments . The third component of the spectra, f_3, decreases from 69.5(5)% for $Al_{0.04}Ga_{0.96}N$ to 41.3(9)% for $Al_{0.77}Ga_{0.23}N$. The significant decrement to 42.7(5)% for $Al_{0.15}Ga_{0.85}N$ is noticeable. Since there is no information about a second component of the probes in samples with intermediate AlN-content, no tendency can be detected.

The QIF of the first fraction, ν_{Q1}, which is proportional to the lattice EFG, increases steeply with rising AlN-content, from 9.42(4) MHz for $x = 0.04$ to 21.4(2) MHz for $x = 0.19$ and then lightly to 30.8(2) MHz for $x = 0.77$. ν_{Q3}, demonstrates the EFGs due to the defects on the probe sites. The related values, ν_{Q3}, grow constantly from 104.2(8) MHz for $x = 0.04$ to 286(10) MHz for $x = 0.77$.

The damping of the first fraction declines from 58.9(6)% to 29.4(7)% as x rises from 0.04 to 0.19 and remains almost constant with further ascending of x. δ_3-values grow from 171(2)% for $x = 0.04$ to 186(12)% for $x = 0.19$, decay sharply to

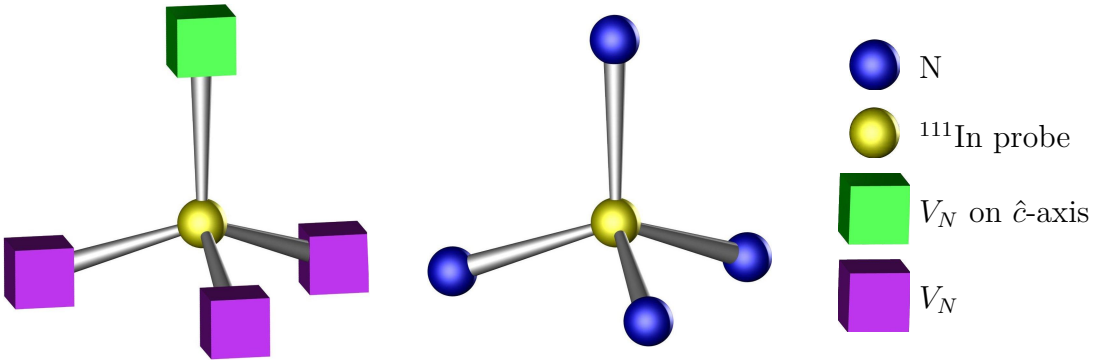

Figure 5.3: *On the left side the possible sites for a V_N is depicted. The previous studies show that In impurities can form a stable complex with V_N aligned with $\hat{c}$-axis [ALV08]. On the right side, the probe is illustrated on the substitutional Al or Ga site of the lattice.*

50(6)% for $x = 0.69$ and stay almost constant until $x = 0.77$. The quantity of δ_3 for $Al_{0.15}Ga_{0.85}N$ is different from the other ones, showing a narrow distribution of the defect EFGs of this sample.

5.1.1 Discussion on AlN-concentration measurements

The first fraction indicates the undisturbed environment of a ^{111}In-probe on a substitutional Al or Ga site. The measurements show that after annealing all the samples at $T_A = 1223\,K$, the lattice with $x = 0.54$ has the most undisturbed environment.

The notable large f_1-value of the sample with 15% AlN-content together with its small defect fraction, are indications of a lattice matched sample. The small δ_3-value shows the narrow distribution of EFGs caused by lattice disorders. The lattice matched properties of AlGaN/GaN grown on sapphire have been observed for $Al_{0.15}Ga_{0.85}N$ by [WOL99]. As expected, the lattice EFG is increasing with AlN-concentrations agreement with previous measurements of ^{181}Hf implanted $Al_xGa_{1-x}N$ [GLV09].

The high frequency of f_2 points out the the lattice defects. The previous studies on AlN and GaN with PAC-probe ^{111}In show that the most probable defect in these alloys is nitrogen vacancy, denoted as V_N. It is energetically favorable for the In impurities to make a complex with a nearest neighbor V_N in the $\langle 0001 \rangle$ position [ALV08].

With $\eta = 0$ for the samples with 4% and 77% AlN-concentration, ν_{Q2}-values show an axial symmetric EFG due to the defects. This can be explained by assuming the V_Ns aligned with the $\hat{c}$-axis. This is in agreement with previous measurements on

GaN and AlN [LRV02] [ALV08]. In contrast, this fraction shows a deviation from axial symmetry in sample with 15% AlN-concentration ($\eta = 0.22(4)$). Therefore, the defects occupy the other sites of the probes in this case (fig. 5.3).

The strongly damped fraction f_3 describes the highly disordered environment of the probes. This can be due to defects on the different possible sites of the probes.

5.2 Temperature dependence of $Al_xGa_{1-x}N$

To study the temperature dependence of $Al_xGa_{1-x}N$, three samples with different AlN-content of 19%, 55% and 77% are used. The implantation and tempering processes are done as explained before. These large and equidistant steps in the Al-concentration provide a good overview over the lattice changes between pure GaN and AlN.

5.2.1 $Al_{0.19}Ga_{0.81}N$ measurements

The temperature dependent $R(t)$ is measured for the $Al_{0.19}Ga_{0.81}N$ sample in the PAC-furnace in vacuum at room temperature, 500 K, 700 K, 850 K and 1000 K. Some of the perturbation functions $R(t)$ measured in PAC-spectroscopy are displayed in fig. C.2.

In order to confirm the reversibility of the defects, the measurement is repeated at 500 K and room temperature.

The spectra can be described as a superposition of two fractions of different probe environments, f_1 and f_2. The data corresponding to each fraction are shown in tab. 5.2, changes of these parameters are illustrated in fig. 5.5.

The first fraction grows with temperature, increasing about 30% between 500 K and 700 K. The second fraction reduces at the same time since $f_2 = 1 - f_1$.

The first fraction's QIF, ν_{Q1} increases lightly from 21.4 MHz at room temperature to 23.8 MHz at 1000 K. The frequency of fraction f_2 decreases as temperature rises and its large decrease between room temperature (155(7) MHz) and 500 K (109(4) MHz) is remarkable, whereas the f_2-values in these temperatures are very close.

The damping of the first fraction, δ_1, stays almost constant while the δ_2-values grow with temperature. The largest damping gradient from 197(9) % at 500 K to 294(11) % at 700 K, denotes the wider distribution of EFGs at higher temperatures.

The results of the remeasurements are shown in fig. 5.5 for room temperature as well as 500 K as *reversed-values* and match the prior values, taking into account the errors.

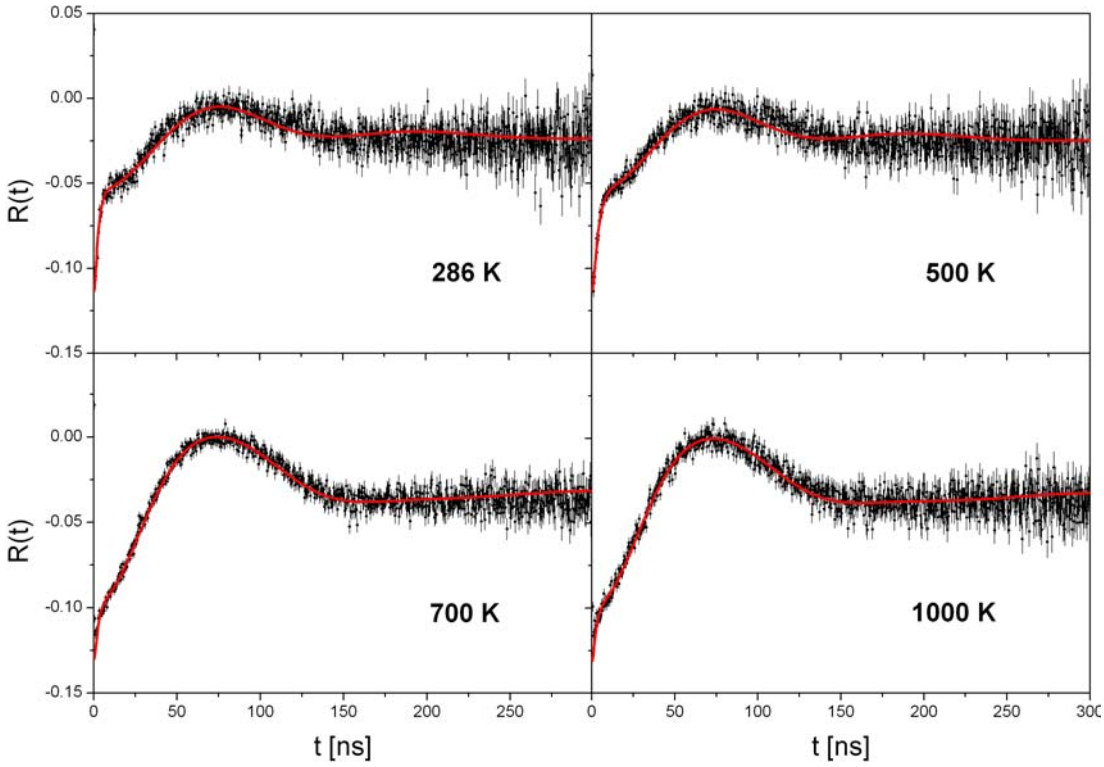

Figure 5.4: *Temperature dependent PAC-spectroscopy of ^{111}In in $Al_{0.19}Ga_{0.81}N$ at selected temperatures. The complete set of spectra can be found in fig. C.2.*

T [K]	286	500	700	850	1000
f_1 [%]	31,2(5)	31,5(6)	61,9(7)	63,9(9)	62,7(9)
ν_1 [MHz]	21,4(2)	21,8(2)	23,62(6)	23,5(1)	23,8(1)
δ_1 [%]	29,4(7)	29,5(8)	26,8(7)	25,8(4)	26,5(4)
f_2 [%]	69(1)	68(1)	38,0(4)	36,1(5)	37,2(5)
ν_2 [MHz]	155(7)	109(4)	105(5)	106(7)	103(6)
δ_2 [%]	186(12)	197(9)	294(11)	299(17)	321(15)

Table 5.2: *Results of PAC temperature dependence measurements for the $Al_{0.19}Ga_{0.81}N$ sample. The measurements are done in the PAC-furnace in vacuum after tempering at $T_A = 1223\,\mathrm{K}$.*
f_1 with low frequency, is set as single crystalline and points out the probes exposed by EFG of the lattice. While f_2 with higher frequency describes the probes on the V_N sites of the lattice and set as polycrystalline.

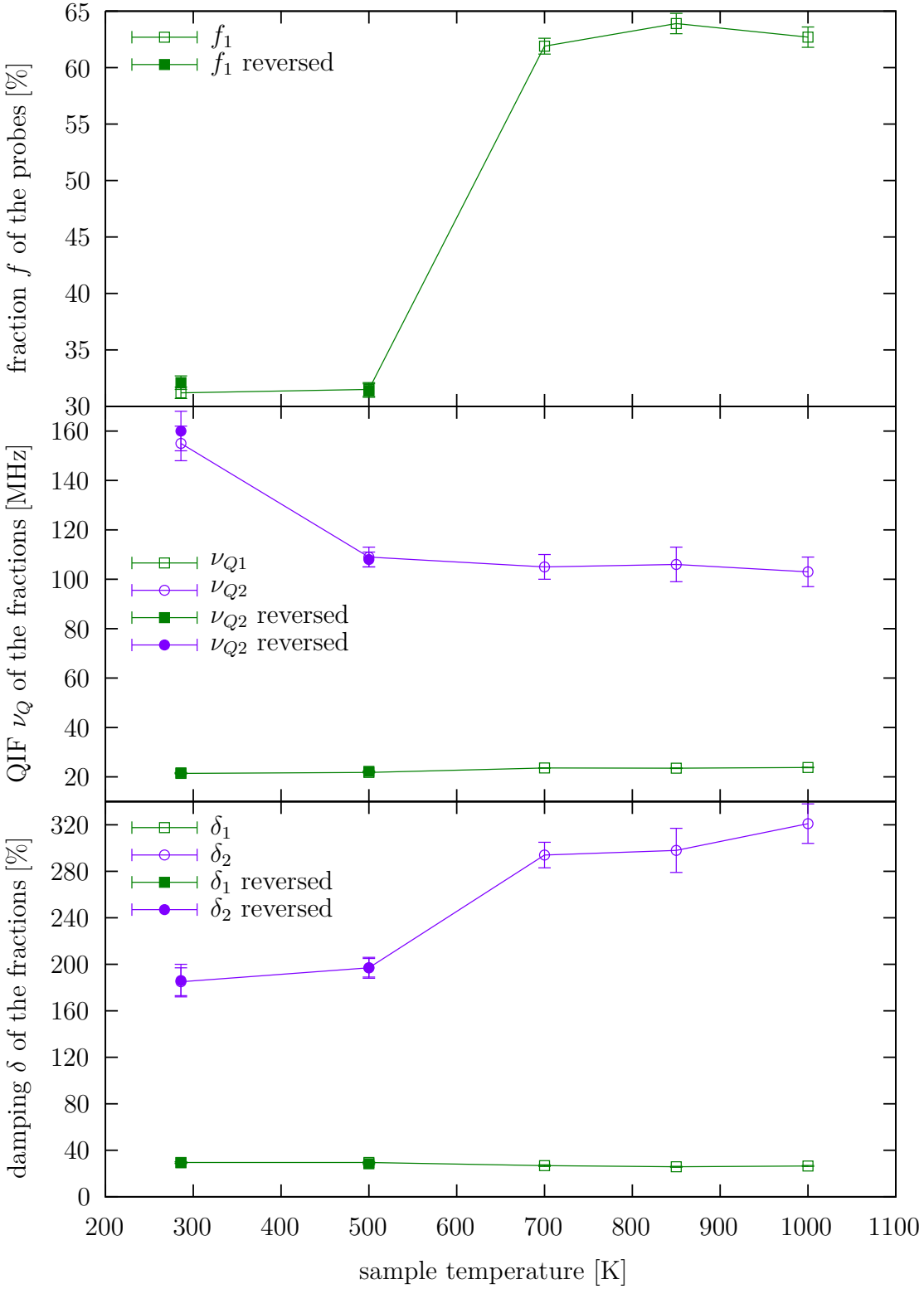
fraction f of the probes [%]
f_1
f_1 reversed
QIF ν_Q of the fractions [MHz]
ν_{Q1}
ν_{Q2}
ν_{Q2} reversed
ν_{Q2} reversed
damping δ of the fractions [%]
δ_1
δ_2
δ_1 reversed
δ_2 reversed
sample temperature [K]

Figure 5.5: *Results of temperature dependence PAC-measurements for the tempered $Al_{0.19}Ga_{0.81}N$ sample ($T_A = 1223\,\mathrm{K}$).*
f_1, with low frequency, shows the probes on the undisturbed lattice sites and is set as single crystalline while f_2, with higher frequency, describes the multi-directional EFGs caused by nitrogen vacancies in the probe sites and is set as polycrystalline.
Reducing ν_{Q2}-values show declining of the EFGs caused by defects. About 30% of the total implanted probes are no more on the disordered environment, rising the temperature from 500 K to 700 K (the upper diagram). At the same temperature step, the damping of the second fraction increases, indicating a wider distribution of EFGs (the middle and the lower diagrams).
The reversed-values, measured for room temperature and 500 K after the measurement at 1000 K, are evidence of reversibility of the results.

Discussion on $Al_{0.19}Ga_{0.81}N$

The first component of the spectra, f_1, can be identified as single crystalline and demonstrates the ^{111}In probes on substitutional lattice sites and its frequency, ν_{Q1} shows the undisturbed, wurtzite structure of the lattice. As it was expected from previous measurements on AlN and GaN, the fraction f_1 increases with temperature. The large jump above 500 K, reveals that at 700 K about 30% of the total implanted probes are not on the disordered environment any more. Above this temperature, f_1 stays almost constant. The slightly rising frequency ν_{Q1} shows increasing of lattice EFG with temperature. This is due to the fact that thermal expansion coefficient of the lattice along $\hat{c}$-axis is larger than that along a- and b-axes [PEN07]. This causes more asymmetry at higher temperatures and leads to larger EFGs. The small damping of this fraction, δ_1, shows the narrow distribution of the lattice frequencies and very well defined environment of the probes.

The second component, f_2, describes the fast frequencies at small times due to V_Ns in the lattice and set as polycrystalline. As the temperature rises, this fraction falls strongly. However, reversed-values at room temperature and 500 K reveal that finding the defect complex in lower temperatures is fully reversible.

5.2.2 $Al_{0.55}Ga_{0.45}N$ measurements

The temperature dependence of $Al_{0.55}Ga_{0.45}N$ sample is measured in a PAC-spectrometer using the PAC-furnace. The measurements are done in vacuum, at different temperatures, varying from room temperature, to 1000 K. Fig. 5.7 illustrates the temperature dependence of the perturbation function $R(t)$.

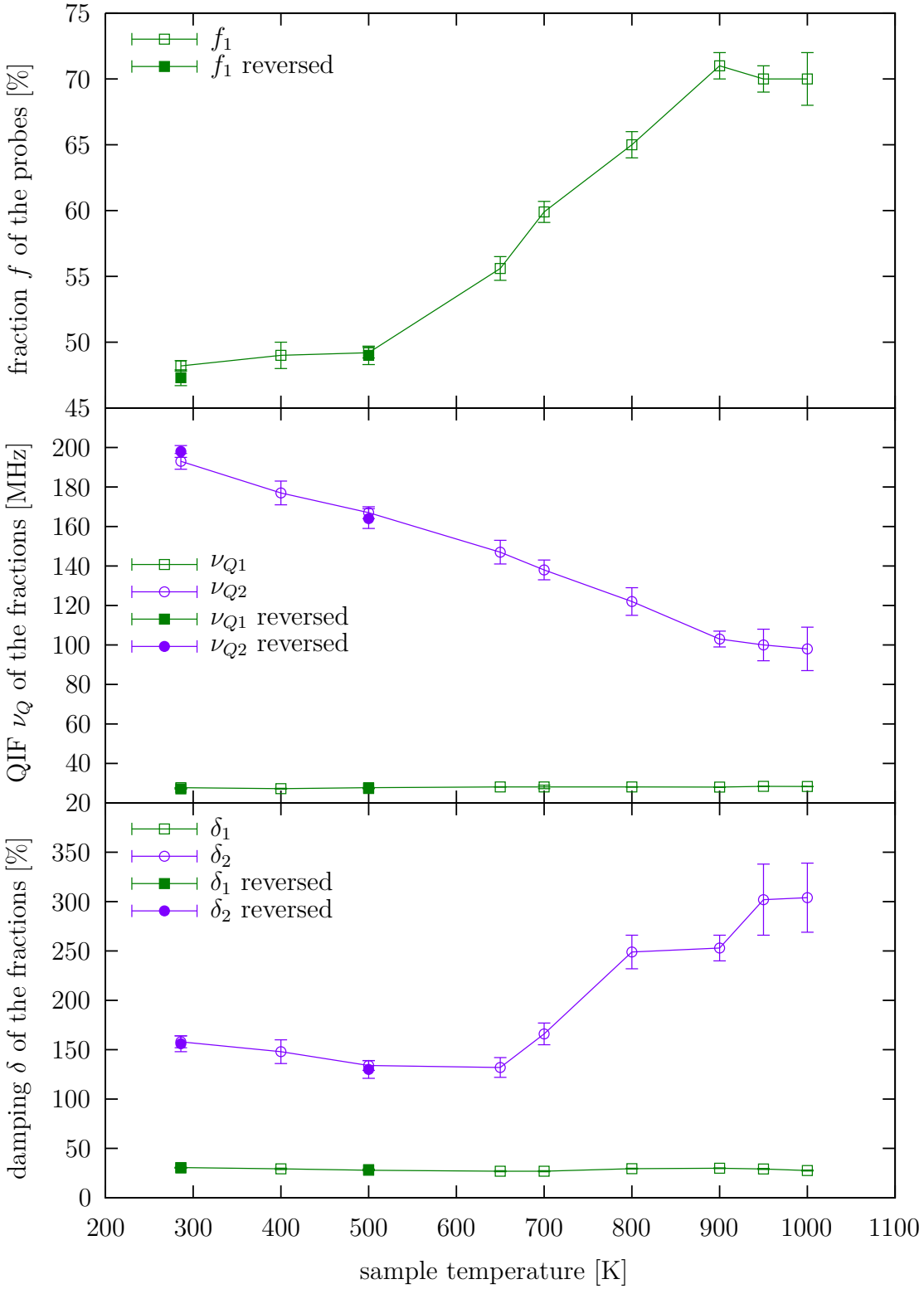
fraction f of the probes [%]
f_1
f_1 reversed
QIF ν_Q of the fractions [MHz]
ν_{Q1}
ν_{Q2}
ν_{Q1} reversed
ν_{Q2} reversed
damping δ of the fractions [%]
δ_1
δ_2
δ_1 reversed
δ_2 reversed
sample temperature [K]

Figure 5.6: *Results of temperature dependence PAC measurements for the $Al_{0.55}Ga_{0.45}N$ sample, after annealing at $T_A = 1223\,\mathrm{K}$. The first fraction, indicating the EFGs due to lattice structure, rises with temperature, showing the annealing of the lattice disorders. The small damping of the first fraction, δ_1, shows the narrow distribution of the corresponding EFGs. f_2, describes the fraction of the probes on V_N sites. ν_{Q2} demonstrates the EFGs due to the lattice disorders which decreases by raising the temperature, showing the annealing of the sample.*
The reversed-values, shown for room temperature and 500 K, are related to the remeasurements done after ascending to 1000 K. Matching the prior values implies the reversibility of the defect complexes.

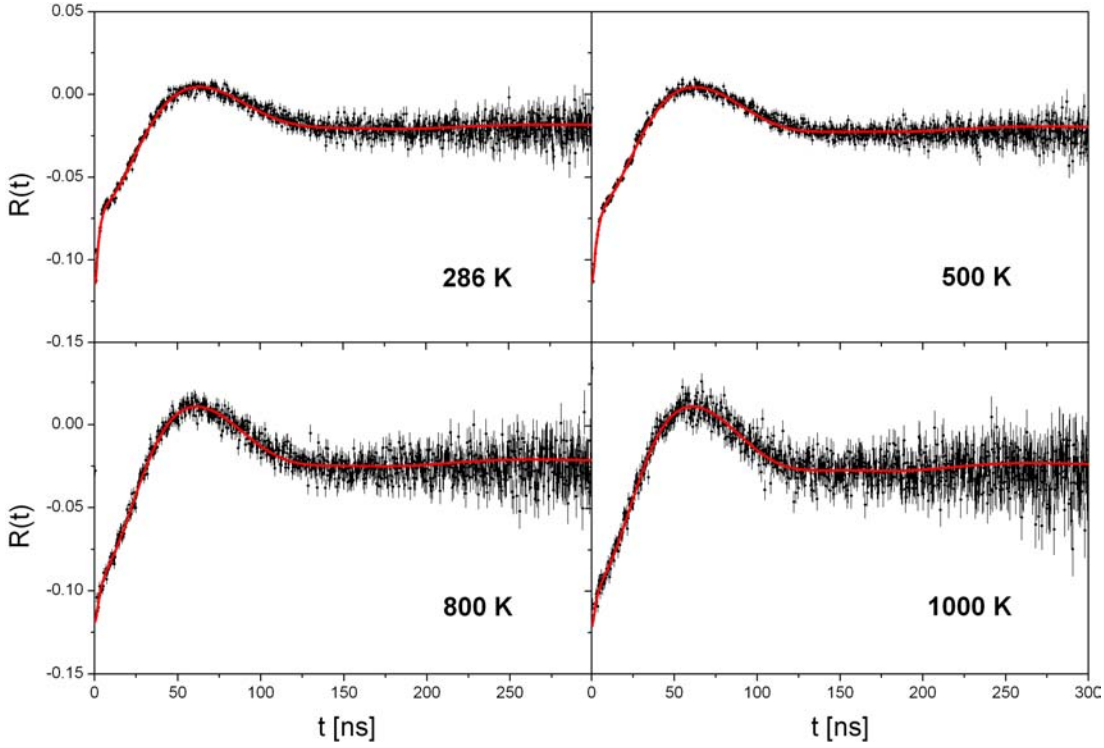

Figure 5.7: *Temperature dependence PAC-spectroscopy of ^{111}In in $Al_{0.55}Ga_{0.45}N$ at some selected temperatures. The complete set of spectra can be found in fig. C.3.*

T [K]	286	500	650	800	950
f_1 [%]	48.2(4)	49.2(4)	55.6(9)	65.3(8)	70(1)
ν_1 [MHz]	27.7(1)	27.7(1)	28.1(1)	28.1(1)	28.4(1)
δ_1 [%]	30.6(4)	27.9(3)	26.9(5)	29.5(4)	29.2(5)
f_2 [%]	52(5)	50.8(4)	44.4(7)	34.7(6)	29.4(7)
ν_2 [MHz]	193(4)	167(3)	147(6)	122(7)	100(8)
δ_2 [%]	158(6)	135(5)	132(10)	249(17)	302(36)

Table 5.3: *Results of PAC temperature dependence measurements for annealed $Al_{0.55}Ga_{0.45}N$ sample ($T_A = 1223\,\mathrm{K}$) at some selected temperatures. The results for all measurements can be found in tab. B.3.*
$R(t)$-functions can be described by two components; a single crystalline fraction,f_1, characterizing the undisturbed lattice with an EFG parallel to the $\hat{c}$-axis, as well as a polycrystalline one, regarding to the disordered environment of the probes.

Once more, to study the reversibility of the results, the ratio functions are remeasured at room temperature and 500 K, after the measurement at 1000 K.

The $R(t)$-spectra are described again as a superposition of two different probe environments: a fraction with low frequency, f_1, describing the probes on undisturbed substitutional Al or Ga sites lattice EFG and a fraction with higher frequency, f_2, demonstrating the probes on the sites of the V_Ns. The corresponding results are shown in tab. 5.3 and fig. 5.6.

The first fraction of the probes increases gradually with temperature from 48.2(4)% at room temperature to 70(1)% at 950 K. The f_1-values rise mostly between 500 K and 900 K where about 20% of the implanted probes are no more on the disordered sites of the lattice. The second fraction decreases respectively, being defined as $f_2 = 1 - f_1$. The asymmetry parameter regarding this fraction, shows the axial symmetry $\eta_1 = 0$.

The QIFs regarding the first fraction, ν_{Q1}, as well as the damping-values, δ_1, stay almost constant at about 28 MHz and 0.29% respectively. In contrast, the ν_{Q2}-values decay strongly from 193(4) MHz at room temperature to 103(4) MHz at 900 K and then stay almost constant. The corresponding dampings decrease from 158(6)% at room temperature to 132(10)% for 650 K and then grow sharply to 249(17)% at 800 K. The δ_2-values increase further from 253(13)% at 900 K to 304(35)% at 800 K.

Discussion on $Al_{0.55}Ga_{0.45}N$

The first component is describing the probes on undisturbed sites of the lattice, and the corresponding low frequency of this fraction, shows the EFGs caused by non-cubic structure of the lattice parallel to $\hat{c}$-axis. The increase of the f_1-values is due to annealing of the crystal at higher temperatures which occurs at high temperature. The δ_1-values do not change notably, implying that the lattice EFGs remains almost the same at higher temperatures. However, decline of the corresponding dampings, δ_1, indicates the narrower distribution of these EFGs at higher temperatures. Unlike to $Al_{0.19}Ga_{0.81}N$, the f_1 does not grow significantly between 500 K and 700 K, the sample heals up gradually from 500 K to 900 K and the fraction of probes at undisturbed sites is still less than $Al_{0.19}Ga_{0.81}N$.

The second fraction, f_2, with higher QIF, describes the fraction of probes at disturbed lattice sites. Being set as polycrystalline, this fraction describes EFGs in various directions in the vicinity of the probes. This suggests the existence of defects at four possible sites of the probes. As the temperature rises, this fraction declines along with its frequency. Strong damping of the fast oscillation, shows the a broad width of EFG distribution at temperatures higher than 800 K.

Alike the before, the measurement is reversible by decreasing the temperature from 1000 K to 500 K and then room temperature. The fit parameters of remeasurements illustrated in fig. 5.6, match the first measurements correctly.

5.2.3 $Al_{0.77}Ga_{0.23}N$ measurements

The temperature dependence of the sample $Al_{0.77}Ga_{0.23}N$ is studied by recording the ratio-function spectra using the PAC-furnace as well. The measurements are performed under vacuum at room temperature and then at temperatures from 500 K to 900 K in steps of 50 K. Some recorded $R(t)$-spectra with corresponding fits are displayed in fig. 5.8.

The orientation measurements (sec. A.1) show that the recorded spectra have to be described by four fractions of different probe environments: two fractions with low frequency and two with higher frequencies (tab. 5.5 and fig. 5.4).

The f_1-values, representing the first fraction, grow with temperature. At room temperature, 16.0(5)% of the implanted probes are on the undisturbed sites of the lattice. This amount stays almost constant till 650 K and then grows regularly (except at 850 K) to 35.5(7)% at 900 K.

The ν_{Q1}-values, proportional to the lattice EFGs, increase slightly from 26.9(3) MHZ at room temperature to 31.4(2) MHZ at 750 K and then decrease slightly to 28.9(1) MHZ at 900 K.

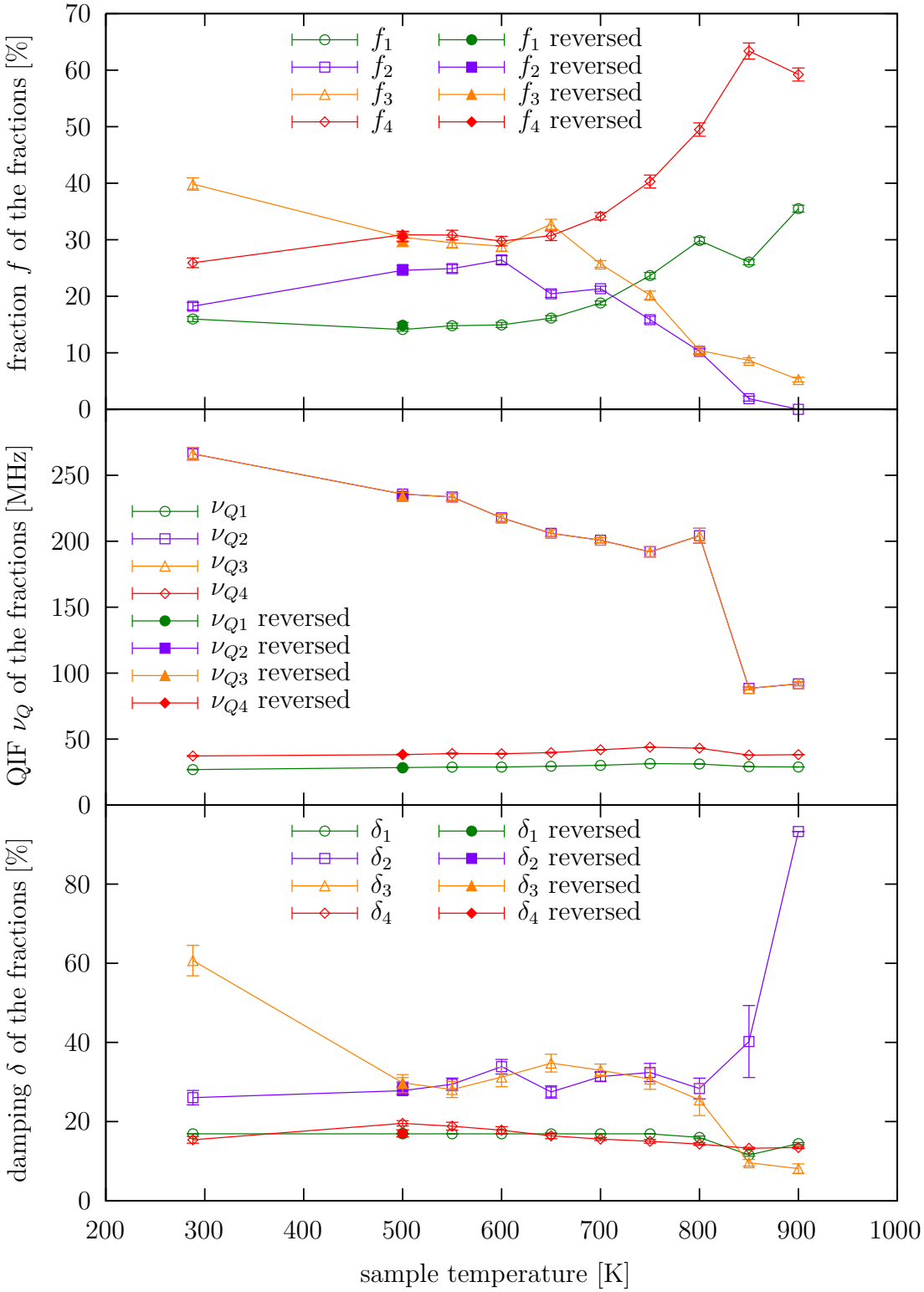
fraction f of the fractions [%]
f_1
f_2
f_3
f_4
f_1 reversed
f_2 reversed
f_3 reversed
f_4 reversed
QIF ν_Q of the fractions [MHz]
ν_{Q1}
ν_{Q2}
ν_{Q3}
ν_{Q4}
ν_{Q1} reversed
ν_{Q2} reversed
ν_{Q3} reversed
ν_{Q4} reversed
damping δ of the fractions [%]
δ_1
δ_2
δ_3
δ_4
δ_1 reversed
δ_2 reversed
δ_3 reversed
δ_4 reversed
sample temperature [K]

Table 5.4: *Results of temperature dependence PAC measurements for the tempered $Al_{0.77}Ga_{0.23}N$ sample ($T_A = 1223\,\mathrm{K}$). The first component, f_1, describes the fraction of the probes at regular lattice sites. f_2 and f_3 with high frequencies, express the probes at the disordered sites of the lattice. The f_4 shows a stronger EFG than the lattice but its similar behavior to f_1 indicates a comparable structure.*
The equal values for ν_{Q2} and ν_{Q3} point out that the EFG caused by the defects in c-direction is the same as the other three sites. The reversed-values show the results of the remeasurement at 500 K.

T [K]	288	550	650	750	850
f_1 [%]	16.0(5)	14.8(5)	16.1(5)	23.7(6)	26.1(5)
ν_1 [MHz]	26.9(3)	28.8(3)	29.4(3)	31.4(2)	26.1(5)
δ_1 [%]	16.9(0)	16.9(0)	16.9(0)	16.9(0)	11.5(4)
f_2 [%]	18.2(7)	24.9(8)	20.4(7)	1.9(5)	1.9(5)
ν_2 [MHz]	226(5)	234(3)	206(3)	192(4)	88(2)
δ_2 [%]	26(2)	29(2)	28(2)	32(3)	40(9)
f_3 [%]	40(2)	30(1)	33(1)	20.2(8)	8.7(5)
ν_3 [MHz]	226(5)	234(3)	206(3)	192(4)	88(2)
δ_3 [%]	61(4)	28(3)	35(3)	31(3)	9.6(9)
f_4 [%]	25.9(9)	30.8(9)	30.7(9)	40(2)	63(2)
ν_4 [MHz]	37.2(4)	39.1(4)	39.7(4)	43.9(3)	37.9(2)
δ_4 [%]	15.4(9)	19(1)	16.4(8)	15.0(5)	13.3(3)

Table 5.5: *Results of temperature dependence PAC-spectroscopy for tempered $Al_{0.77}Ga_{0.23}N$ ($T_A = 1223\,\mathrm{K}$) at some selected temperatures. The results for all the measurements can be found in tab. B.1.*
The ratio functions are described by a superposition of four components. The first two components, f_1 and f_2, are set as single crystalline where the former with low frequency denotes the undisturbed lattice EFG parallel to $\hat{c}$-axis and the latter shows the lattice disorder in c-direction. The third component is set as polycrystalline and demonstrates multi-directional EFGs in the lattice caused by defects with other orientations. The fourth fraction is also set as polycrystalline and its behavior is similar to the f_1.

The second and third fractions of the probes decrease with raising the temperature, and have the same QIFs, giving the hint that f_2 and f_3 are describing the probes at the defect sites of the lattice. The second fraction is set to single crystalline and has axial symmetry ($\eta = 0$), describing the defects in c-direction while the third one is set to polycrystalline, denoting lattice defects at the other sites.

The second fraction first rises from 18.2(7)% at room temperature to 26.4(8)% at 600 K and then decreases to 0(0)% at 900 K. The third fraction declines almost constantly from 40(2)% at room temperature to 5.3(5)% at 900 K.

The QIFs ν_{Q2} and ν_{Q3} have the same values and are decreasing as the temperature rises.

The damping of the the first and fourth fractions decrease similarly with rising temperature. Though, the second and third fractions with the same frequencies, have different damping behaviors. δ_2 remains almost constant till 800 K and then rises sharply to 93.3(5)% at 900 K. In contrast, δ_3 decreases significantly from 61(4)% at room temperature to 30(2)% at 500 K and then remains almost constant to 800 K and then declines again to 8(2)% at 900 K.

The results of remeasurement at 500 K show the reversibility of the measurement.

Discussion on $Al_{0.77}Ga_{0.23}N$

Rising the AlN-content of the alloy to 77%, the spectra can not be described by two components. Two of the fractions f_1 and f_4 however, behave similarly and two other fractions have the same QIFs.

Analogous to the previous samples, the first fraction, f_1, describing the probes exposed to the undisturbed lattice EFG in c-direction ($\eta = 0$), increases with rising temperature. The slightly rising lattice EFG is due to different expansion constant in c-direction while the decreasing between 800 K and 900 K shows the overcoming of expansion factor which causes a longer bonding lengths and consequently a weaker EFG [PEN07].

The relative low frequency of the forth fraction, together with its similar behavior to the lattice fraction, can indicate existence of single crystalline clusters with different orientated $\hat{c}$-axis.

The second and third fractions are describing the EFGs caused by lattice defect on four possible sites of the probes. The second fraction with $\eta = 0$ denotes the defects in the c-direction while the third one set as polycrystalline, shows the defects in the all possible directions. Decreasing defect EFG with rasing temperature, shows the expansion of the lattice.

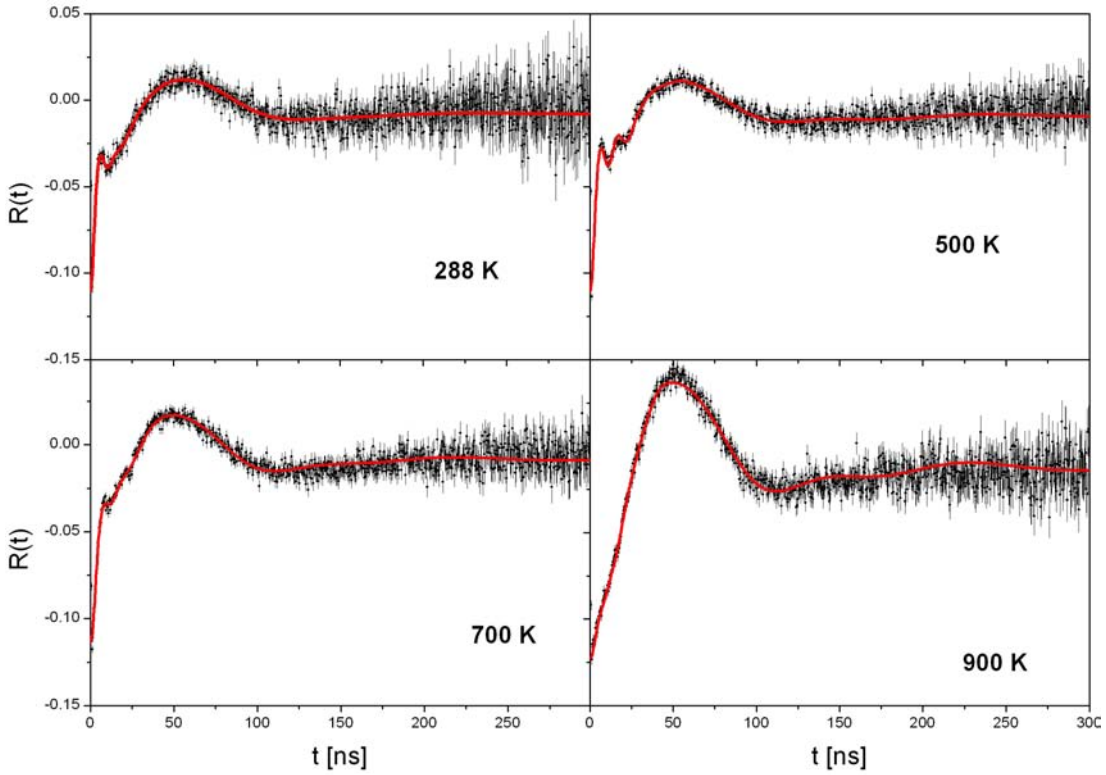

Figure 5.8: *Temperature dependence PAC-spectroscopy of ^{111}In in $Al_{0.77}Ga_{0.23}N$ at some selected temperatures. The complete set of recorded spectra can be found in fig. C.4.*

5.2.4 Discussion on Temperature dependence of $Al_xGa_{1-x}N$

The results of temperature dependent $Al_xGa_{1-x}N$ measurements for $x = 0.19$ and $x = 0.55$ (shown in fig. 5.10) are in agreement with the previous studies on GaN and AlN by [SCH07]. The results show an EFG caused by the lattice in $\hat{c}$-direction ($\eta \approx 0.05$) and an EFG due to the V_Ns on the probes' sites. The fraction of the probes at substitutional Al or Ga sites grows as the temperature rises and the lattice EFG increases with AlN-concentration. The damping of the lattice EFG stays almost constant due to the dislocations which is inherent in ternary alloys.

The defect QIF decreases with temperature. This can be explained by expansion of the lattice (fig. 5.9). Moreover, the axial symmetric defect EFG is found for the sample with 77% AlN-content suggesting the V_Ns are aligned with the $\hat{c}$-axis.

The sample with 77% AlN-concentration, however, can not be fully described only with two fractions. The orientation measurements show two EFGs which have no specific orientations. The one with fast frequency points out the V_Ns which are

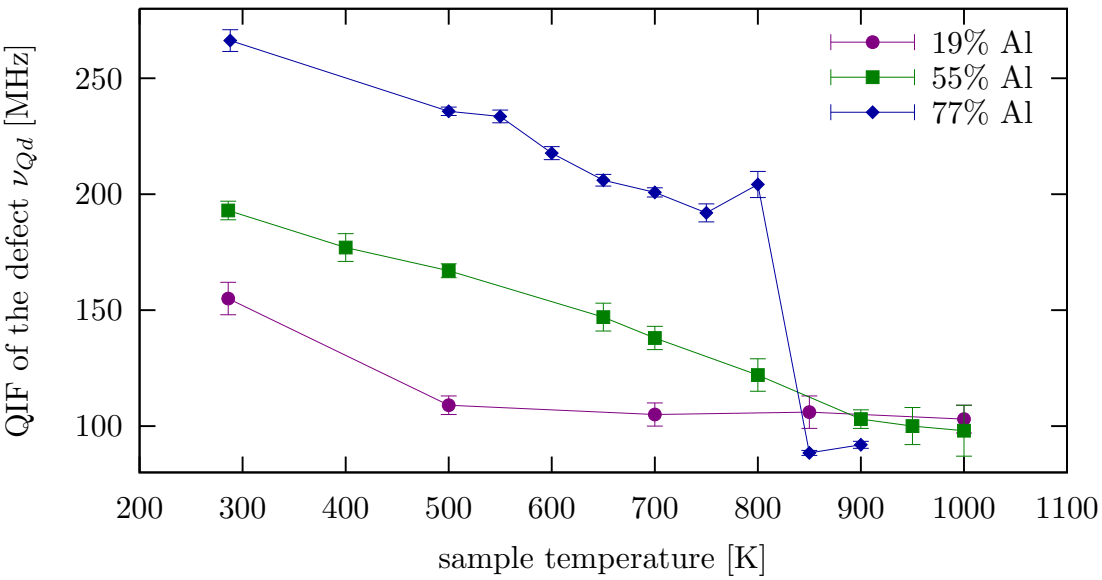

Figure 5.9: *Comparison of the defect QIF in temperature dependent measurements of $Al_xGa_{1-x}N$ alloys with different AlN-concentrations.*

not aligned with the $\hat{c}$-axis, while the other fraction with a QIF of about 39 MHZ, behaves the same as the undisturbed lattice fraction. One possible explanation is existence of single crystalline clusters in the sample, with different orientations.

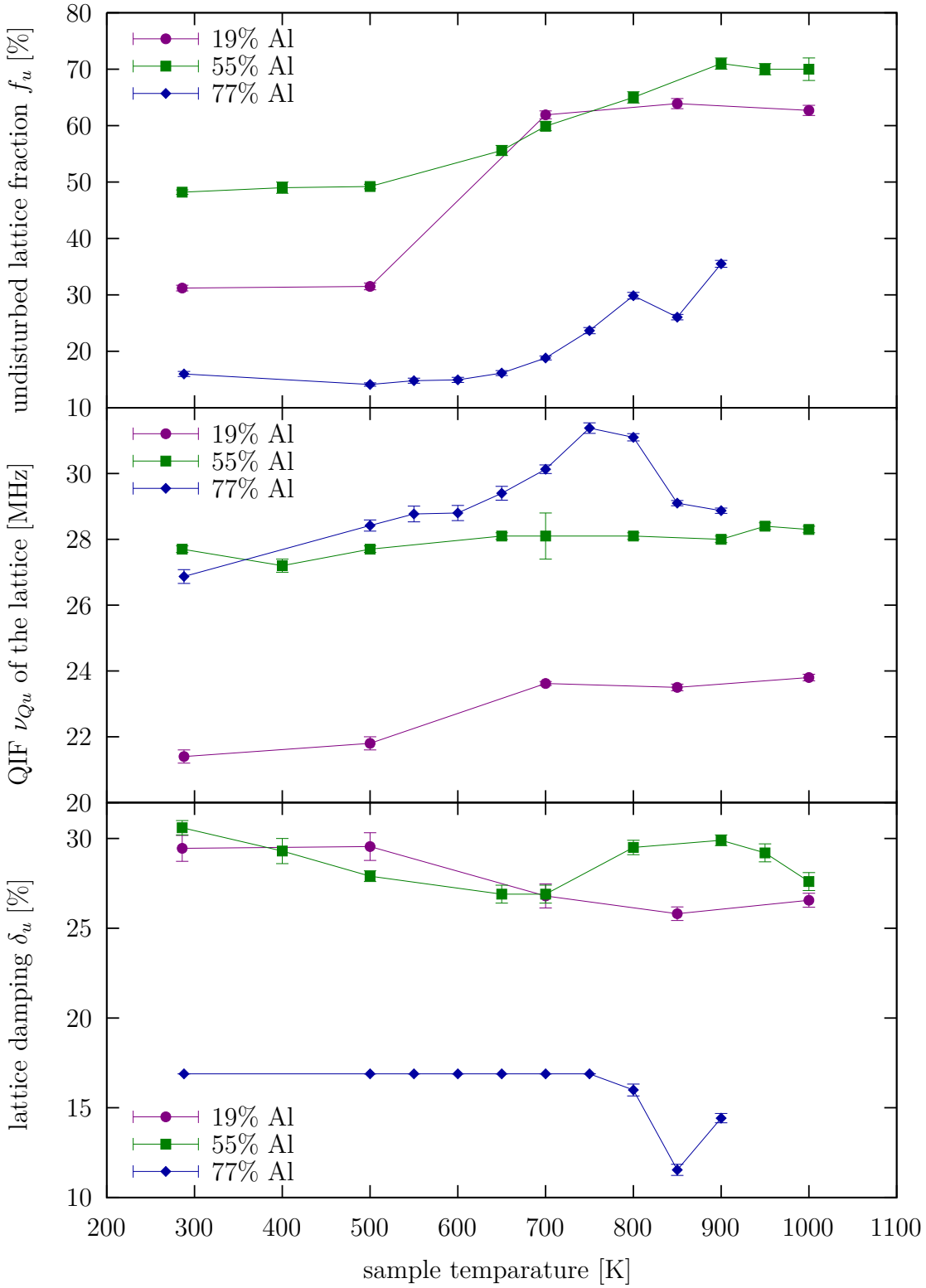

Figure 5.10: *Comparison of the lattice fraction in temperature dependent measurements of $Al_xGa_{1-x}N$ alloys with different AlN-concentrations.*

6. Measurements of $In_xAl_{1-x}N$

To study the ternary semiconductor $In_xAl_{1-x}N$, three 100 nm thick samples with $x = 0.12$, $x = 0.17$ and $x = 0.21$ are used. Despite the Al is the major group III element in these samples, the possible effects of slight changes of AlN-content is of experimental interest; hence, the samples are described by In-content index, x.

6.1 Tempering

To study the tempering behavior of $In_xAl_{1-x}N$, the three samples are implanted with ^{111}In under 7° with an energy of 40 keV and tempered in different temperature steps. The first sample, with $x = 0.21$, is measured after implantation and then after tempering stemps of 500 K, 700 K, 900 K and 1000 K under nitrogen atmosphere for 120 s. The spectra shown in fig. 6.1, denote a highly damaged lattice after implantation and after tempering at 1000 K.

T [K]	298	500	700	900	1000
ν_Q [MHz]	94(1)	84.4(7)	82.4(4)	76.5(6)	79.6(5)
δ [%]	42(1)	41.9(7)	50.2(5)	46.6(7)	51.2(6)

Table 6.1: *Results of PAC-measurements of $In_{0.21}Al_{0.79}N$ after each tempering step. The measurement at 298 K is performed without prior annealing called as implanted.*

The spectrum is described as a polycrystalline environment of the lattice since the orientation measurements show no preferred direction of the defects. The results are shown in tab. 6.1. The corresponding EFGs decrease from 94(1)% to 76.5(6)% as the T_A is raised from room temperature to 900 K. The slightly increasing damping shows the broad distribution of the EFGs becomes wider. Increasing of the QIF in the last step of tempering is regardless to the trend and can be caused by the highly damaged environment of the probes due to too high annealing temperatures.

The second sample with $x = 0.17$ together with the third one ($x = 0.12$) is measured after implantation as well as tempering steps of 500 K, 700 K and 900 K.

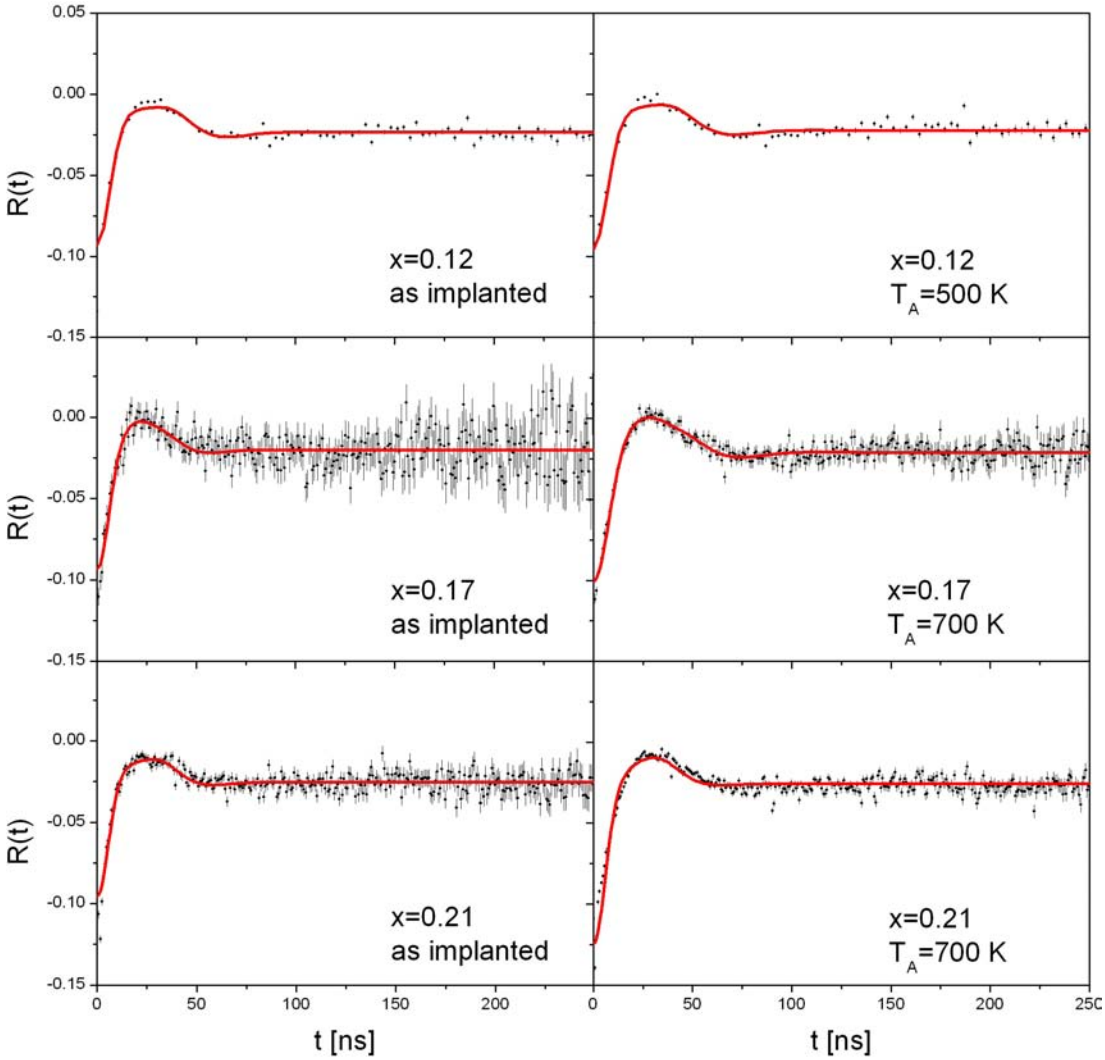

Figure 6.1: *PAC-spectroscopy of ^{111}In in $In_xAl_{1-x}N$ after the corresponding annealing steps.*

To avoid damaging the samples, tempering process is not done at 1000 K for these samples.

T [K]	298	500	700	900
ν_Q [MHz]	86(2)	80(1)	67.6(6)	65.4(6)
δ [%]	42(1)	41(1)	37.5(8)	35.7(8)

Table 6.2: *Results of PAC-measurements of $Al_{0.83}In_{0.17}N$ after each tempering step. The measurement at 298 K is performed without prior annealing called as implanted.*

The spectra are described as polycrystalline environment of the probes and the obtained results shown in tab. 6.2 and 6.3. Like the first sample, the QIF falls as the T_A is raised while it is much higher than the specific QIFs of AlN ($\nu_Q = 28.8(3)$) and InN ($\nu_Q = 22.4(2)$)recording to [SCH07]. The ν_Q values therefore, give no information about the lattice EFG.

Comparing the recorded spectra of each sample, it is deduced that the lattice in samples with $x = 0.21$ and $x = 0.17$ are best recovered by tempering at 700 K, however the lattice in sample with smaller In-content, $x = 0.12$, is best recovered at 500 K. The PAC-spectroscopy are shown in fig. XXX for the measurements after implantation as well as the best recovered ones. REFERENCE!

T [K]	298	500	700	900
ν_Q [MHz]	86.0(6)	87.4(6)	78.6(5)	80.4(8)
δ [%]	37.2(6)	39.1(6)	38.7(6)	39.9(9)

Table 6.3: *Results of PAC-measurements of $Al_{0.88}In_{0.12}N$ after each tempering step. The measurement at 298 K is performed without prior annealing called as implanted.*

6.2 Temperature dependence

Temperature dependence of the $In_xAl_{1-x}N$ is studied for the sample with $x = 0.17$ In-content. After implantation, it is tempered at $T_A = 500$ K in the RTA-unit and measured in vacuum, using PAC-furnace. The measurements are done at room temperature and from 500 K to 850 K in 50 K steps. The measurement is not done at higher temperatures since the annealing results show that the crystal is damaged about 900 K.

The orientation measurement implies that the spectra can be described by a polycrystalline probe environment. The results of the measurements are shown in

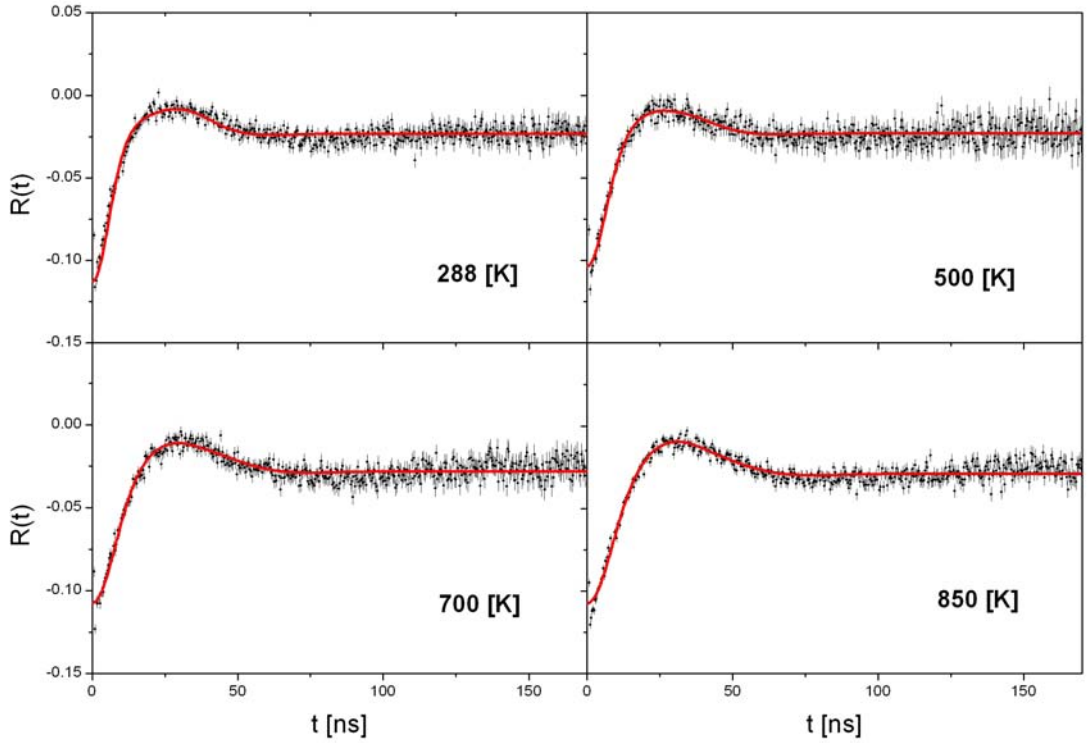

Figure 6.2: *Temperature dependence PAC-spectroscopy of ^{111}In in $In_{0.17}Al_{0.83}N$ at some selected temperatures.*

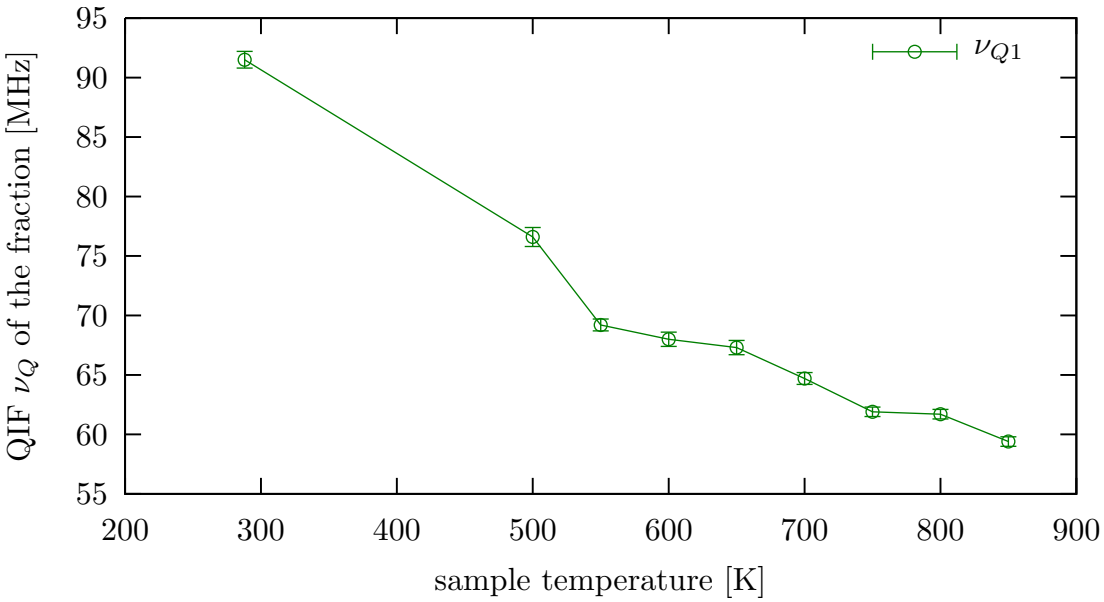

Figure 6.3: *Results of temperature dependence PAC-measurements for tempered $In_{0.17}Al_{0.83}N$ sample ($T_A = 500\,\mathrm{K}$). The spectra is described by a polycrystalline fraction of the probes illustrating the probes at V_N sites of the lattice. The EFGs decrease almost linearly as the temperature rises.*

fig. 6.3. The QIF declines almost linearly as the temperature rises, denoting the smaller EFGs in the lattice. The damping of the oscillation is almost constant about 48% and shows a consistent distribution of the field gradients.

6.2.1 Discussion

The temperature treatment measurements show that the annealing temperature is higher for the samples with more InN-content.

The measured EFGs for the $In_xAl_{1-x}N$ samples show no specific direction for the EFGs in the lattice according to the orientation measurements (A.3). This points out that it is energetically favorable for the V_Ns to occupy all the four possible sites of the tetrahedrons.

The measured QIFs are much higher than the previous results for the lattice EFG in AlN (e.g. [SCH07]). On the other hand, the decreasing QIF in the temperature dependent measurements refers to the typical defect behavior in the wurtzite structure. This indicates a high degree of disorder at the lattice.

The broad frequency distribution in temperature dependent results is consistent with tempering ones and has been observed in InN measurements as well [DSB05]. This is another evidence for a diverse set of different defects in the atomic scale.

7. Summary and conclusion

The current work concerns the application of PAC-technique to investigating the lattice disorder and temperature dependence of ^{111}In implanted ternary alloys $Al_xGa_{1-x}N$ and $In_xAl_{1-x}N$.

The measurements on $Al_xGa_{1-x}N$ samples with different AlN-concentrations are performed after implantation and annealing. The results show a continuous change from the lattice frequency range of GaN to AlN. In the samples with small(large) AlN-content ($x = 0.04$ and $x = 0.77$), the In-V_N defect is aligned with $\hat{c}$-axis. However, in the alloys with intermediate AlN-content, the defect has no preferred orientation and the defect QIF can be described as a multi-directional EFG. This can be due to the dislocations caused by different atom radii of Ga and Al.

The measurement results in an alloy with 15% AlN-concentration which is lattice-matched to its sapphire substrate, show a significant increase in the undisturbed fraction and a reduction of the damping parameter.

The temperature dependence of three $Al_xGa_{1-x}N$ samples with 19%, 55% and 77% AlN-concentration are studied. The lattice QIF increases slightly due to the different expansion constants, however, the defect EFG decreases considerably. The fraction of probes at the regular lattice site in the sample with 55% AlN-content is larger than in the one with 19% AlN-content. Nevertheless, this fraction decreases notably in the sample with 77% AlN-content. The results show that in this alloy a large fraction of probes are exposed to a EFG which is stronger than the lattice EFG but correlated with it. This can be due to single crystalline clusters with different orientations. Furthermore, the high dislocation density may cause such an effect. However, more orientation measurements have to be performed to fortify these assumptions.

The reversibility of the local structure of of the probes is studied in temperature dependent measurements. The results of the measurements are completely reversible after the measurements at high temperature.

An alteration of the annealing behavior of $In_xAl_{1-x}N$ due to InN-content variation is studied and the appropriate annealing temperatures for samples with different compositions are determined. The In-V_N complex is not observed, presumably due to the large amout of stable In which acts as a competing trap for V_N.

Appendix

A. Orientation measurements

Considering the sample as single crystalline, the perturbation function is affected not only by the direction of γ_1, but also by the orientation of the lattice-EFG with respect to the detectors. The general geometry of the measurement's arrangement together with the orientation of the field gradient V_{zz}, are packed in the weights of cosine functions, $s_{nN}^{k_1 k_2}$, shown in eq. (3.17). In this way, depending on the measurement's arrangement, a cosine function can be weighted more than the others and the corresponding frequency can be observed distinctly in the recorded $R(t)$-function.

In the present work, all measurements are done in 45° geometry, except the orientation measurements. In this arrangement, the $\hat{c}$-axis of the sample is in the detectors' plane and makes an angle of 45° or 135° with the detectors (fig. A.1 above, left). If the EFG is parallel to the $\hat{c}$-axis, the second transition frequency, ω_2, is weighted more than the other frequencies and the $R(t)$-function shows mainly a modulation of ω_2 (fig. A.1 below, left).

If the EFG is directed at a start-detector (fig. A.1 above, middle), no interaction can be observed since all transition frequencies are eliminated through the orientation. The ratio function is collapsed to a constant value (fig. A.1 below, middle).

In another case, if the EFG is perpendicular to the start-detector (fig. A.1 above, right), the first transition frequency, ω_1, is weighted more, as it is shown for ^{111}In in fig. A.1 lower graph, right, where $\omega_2 = 2\omega_1$ (and therefore the period is twice the one in the 45° geometry.)

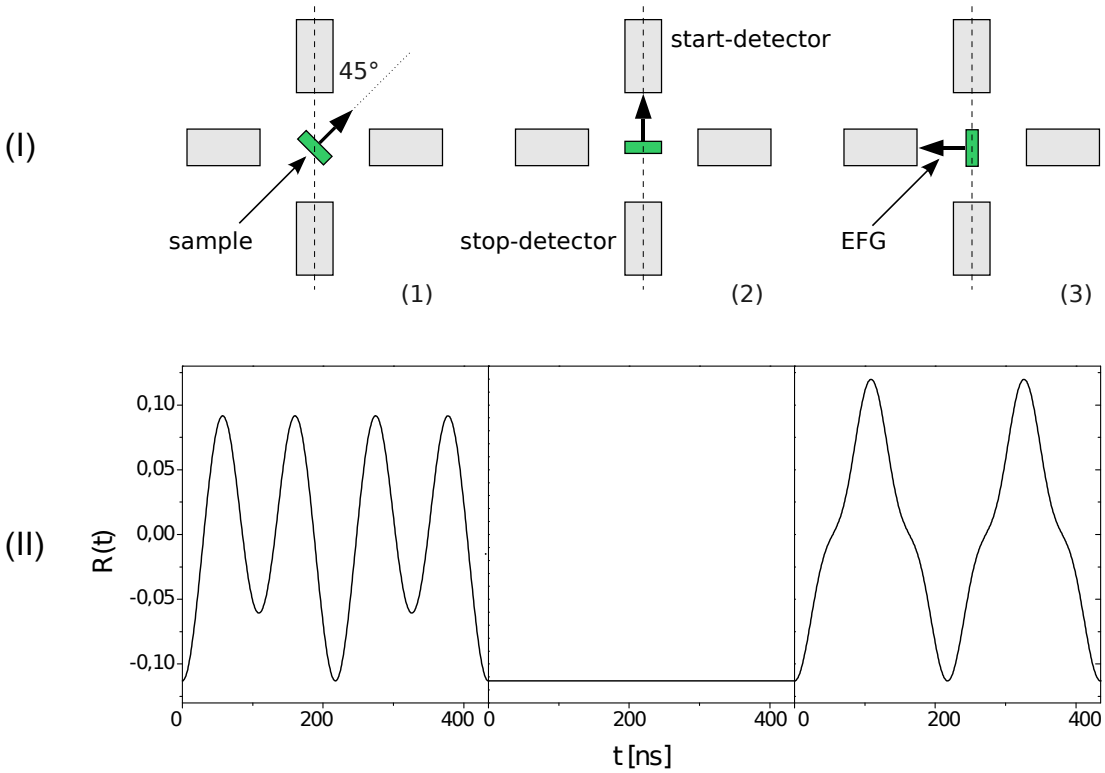

Figure A.1: *(I): Different orientations of the EFG with respect to the start-detector; left: 45° geometry, middle: directed at the start-detector, right: perpendicular to the start-detector.*
(II): Simulation of the $R(t)$-spectra belonging to the above orientations

A.1 Orientation measurements of $Al_{0.77}Ga_{0.23}N$

Before temperature dependent measurements are performed, the $Al_{0.77}Ga_{0.23}N$ sample is measured in different alignments of its $\hat{c}$-axis, at room temperature. The orientation of the EFGs in different environments of the probes can be obtained from this measurement. The $R(t)$-spectra are shown in fig. A.2.

To describe the spectra in which the $\hat{c}$-axis of the sample is perpendicular to the start-detector (fig. A.2, right), four fractions of probes are needed: two single crystalline fractions and two polycrystalline ones. The single crystalline fractions representing the probes on undisturbed environments and ^{111}In-V_N defects along $\langle 0001 \rangle$ direction, are not observed in the results of parallel geometry (fig. A.2, left). However, two other polycrystalline fractions with QIFs of 271(6) MHz and 41.7(6) MHz appear in the $R(t)$-spectra. This indicates the existence of four different probe environments.

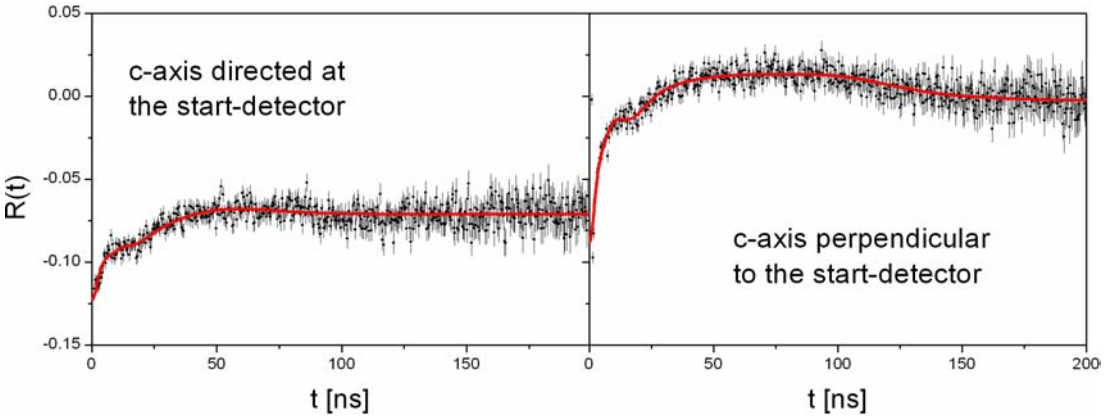

Figure A.2: *Orientation measurements of AlGaN using the annealed sample with 77% AlN-content ($T_A = 1223\,\mathrm{K}$).*

A.1.1 Orientation measurements of $In_{0.17}Al_{0.83}N$

After implanting ^{111}In under 7° with an energy of 60 keV, the $In_{0.17}Al_{0.83}N$ sample is tempered at $T_A = 500\,\mathrm{K}$. Before temperature dependent measurements are done, the sample is measured in different alignments of its $\hat{c}$-axis, at room temperature. The $R(t)$-spectra are shown in fig. A.3.

The spectra are almost the same for all of the three arrangements and point out that the EFGs in the lattice have no specific direction. The V_Ns therefore, can be found on the four possible sites, with the same probability.

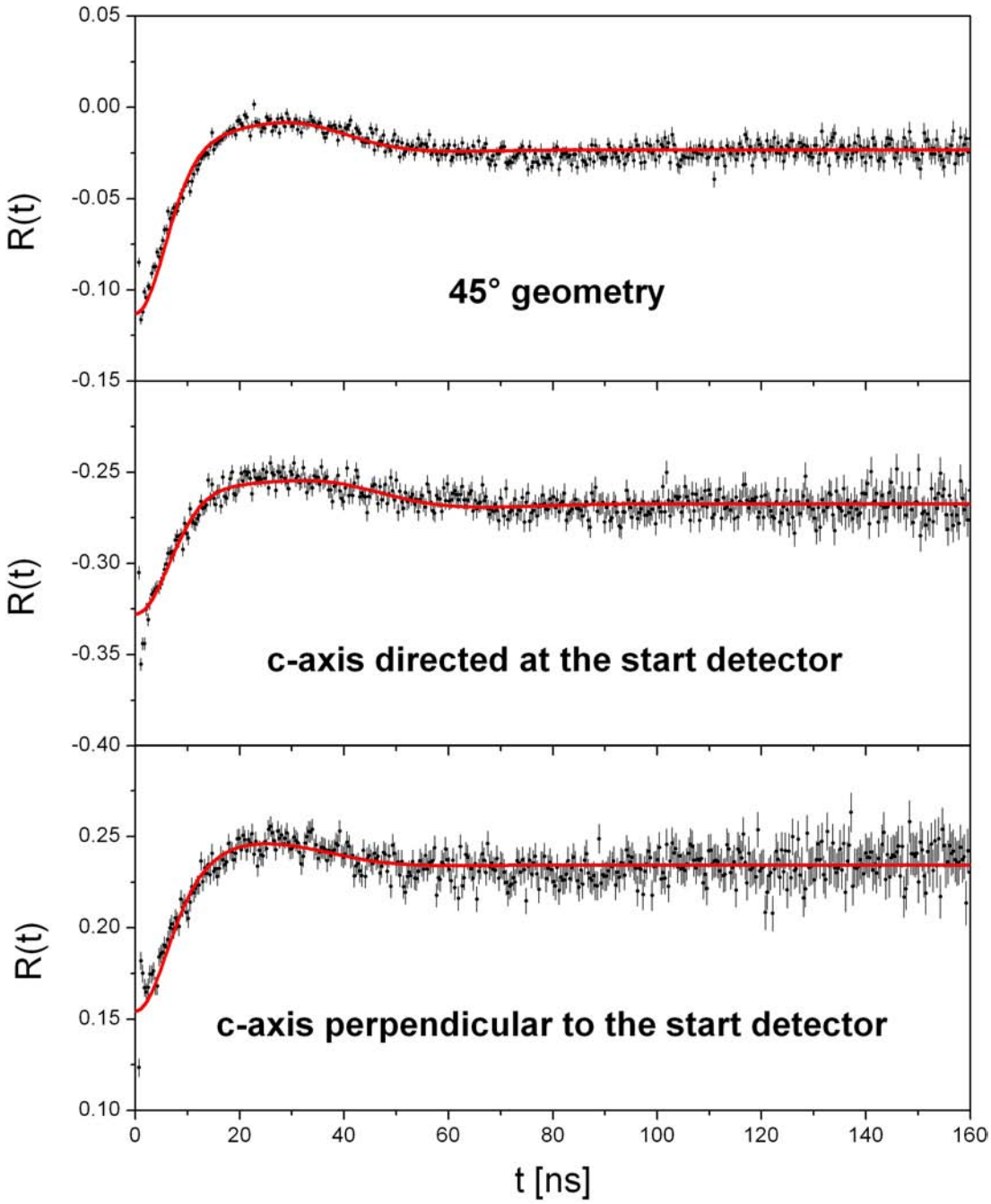

Figure A.3: *$R(t)$ spectra of $In_{0.17}Al_{0.83}N$ with different orientations. The spectra show the same frequency in different arrangements indicating that the orientation of field gradients in the lattice is independent of the $\hat{c}$-axis.*

B. Tables

T [K]	288	500	550	600	650
f_1 [%]	16.0(5)	14.1(3)	14.8(5)	15.0(5)	16.1(5)
ν_1 [MHz]	26.9(3)	28.4(2)	28.8(3)	28.8(3)	29.4(3)
δ_1 [%]	16.9(0)	16.9(0)	16.9(0)	16.9(0)	16.9(0)
f_2 [%]	18.2(7)	24.6(3)	24.9(8)	26.4(8)	20.4(7)
ν_2 [MHz]	226(5)	236(2)	234(3)	218(3)	206(3)
δ_2 [%]	26(2)	28(1)	29(2)	34(2)	28(2)
f_3 [%]	40(2)	30.4(7)	30(1)	29(1)	33(1)
ν_3 [MHz]	226(5)	236(2)	234(3)	218(3)	206(3)
δ_3 [%]	61(4)	30(2)	28(3)	31(3)	35(3)
f_4 [%]	25.9(9)	30.9(6)	30.8(9)	29.8(9)	30.7(9)
ν_4 [MHz]	37.2(4)	38.2(3)	39.1(4)	38.9(4)	39.7(4)
δ_4 [%]	15.4(9)	19.5(7)	19(1)	17.8(9)	16.4(8)
T [K]	700	750	800	850	900
f_1 [%]	18.8(4)	23.7(6)	29.9(6)	26.1(5)	35.5(7)
ν_1 [MHz]	30.1(2)	31.4(2)	31.1(2)	29.1(1)	28.9(1)
δ_1 [%]	16.9(0)	16.9(0)	16.0(4)	11.5(4)	14.4(3)
f_2 [%]	21.3(5)	15.9(6)	10.3(5)	1.9(5)	0.0(0)
ν_2 [MHz]	201(2)	192(4)	204(6)	88(2)	92(2)
δ_2 [%]	31(2)	32(3)	28(3)	40(9)	93.3(5)
f_3 [%]	25.7(6)	20.2(8)	10.4(6)	8.7(5)	5.3(5)
ν_3 [MHz]	201(2)	192(4)	204(6)	88(2)	92(2)
δ_3 [%]	33(2)	31(3)	26(4)	9.6(9)	8(2)
f_4 [%]	34.2(7)	40(2)	50(2)	63(2)	59(2)
ν_4 [MHz]	41.9(2)	43.9(3)	43.1(2)	37.9(2)	38.2(2)
δ_4 [%]	15.6(4)	15.0(5)	14.3(4)	13.3(3)	13.4(3)

Table B.1: *Results of temperature dependence PAC-measurements for tempered* $Al_{0.77}Ga_{0.23}N$ *(*$T_A = 1223\,\mathrm{K}$*)*

Al content x	0	0.04	0.15	0.19
f_1 [%]	48.5(7)	27.3(2)	39.2(3)	31.2(5)
ν_{Q1} [MHz]	6.9(1)	9.42(4)	17.34(4)	21.4(2)
δ_1 [%]	0	58.9(6)	36.4(4)	29.4(7)
f_2 [%]	20.3(3)	3.2(1)	18.0(3)	–
ν_{Q2} [MHz]	74(7)	106.1(9)	266.3(3)	–
δ_2 [%]	77(11)	11.2(8)	22(1)	–
f_3 [%]	31.2(8)	69.5(5)	42.7(5)	68.8(7)
ν_{Q3} [MHz]	10.5(1)	104.2(8)	125(2)	155(7)
δ_3 [%]	28(1)	171(2)	53(1)	186(12)
Al content x	0.54	0.69	0.77	1
f_1 [%]	47.2(8)	43(2)	38.2(6)	23.9(7)
ν_{Q1} [MHz]	27.3(4)	26.3(7)	30.8(2)	28.9(3)
δ_1 [%]	31.0(7)	34.0(2)	28.3(8)	2.6(2)
f_2 [%]	–	–	20.4(7)	23.9(9)
ν_{Q2} [MHz]	–	–	287(5)	138(4)
δ_2 [%]	–	–	27(2)	13.2(9)
f_3 [%]	52.9(8)	57(3)	41.3(9)	51(1)
ν_{Q3} [MHz]	188(7)	223(15)	286(10)	34.4(4)
δ_3 [%]	82(5)	50(6)	58(4)	8.5(2)

Table B.2: *Results of PAC-measurements for annealed $Al_xGa_{1-x}N$ samples ($T_A = 1223\,\mathrm{K}$) depending on the AlN-content.*
Results of of AlN and GaN are from [NIE09] [SCH07] and shown for comparison. The third fraction of the corresponding result has been set as single crystalline and can not be compared with the other results.

T [K]	286	400	500	650	700
f_1 [%]	48.2(4)	49(1)	49.2(4)	55.6(9)	59.9(8)
ν_1 [MHz]	27.7(1)	27.2(2)	27.7(1)	28.1(1)	28.0(9)
δ_1 [%]	30.6(4)	29.3(7)	27.9(3)	26.9(5)	26.9(5)
f_2 [%]	52(5)	51(1)	50.8(4)	44.4(7)	40.1(5)
ν_2 [MHz]	193(4)	177(6)	167(3)	147(6)	138(5)
δ_2 [%]	158(6)	148(12)	135(5)	132(10)	166(11)
T [K]		800	900	950	1000
f_1 [%]		65.3(8)	71(1)	70(1)	70(1)
ν_1 [MHz]		28.1(1)	28.01(7)	28.4(1)	28.3(1)
δ_1 [%]		29.5(4)	29.9(3)	29.2(5)	27.6(5)
f_2 [%]		34.7(6)	29.0(4)	29.4(7)	29.5(7)
ν_2 [MHz]		122(7)	103(4)	100(8)	98(11)
δ_2 [%]		249(17)	253(13)	302(36)	304(35)

Table B.3: *Results of PAC temperature dependence measurements for tempered $Al_{0.55}Ga_{0.45}N$ sample ($T_A = 1223\,\mathrm{K}$).*

C. Spectra

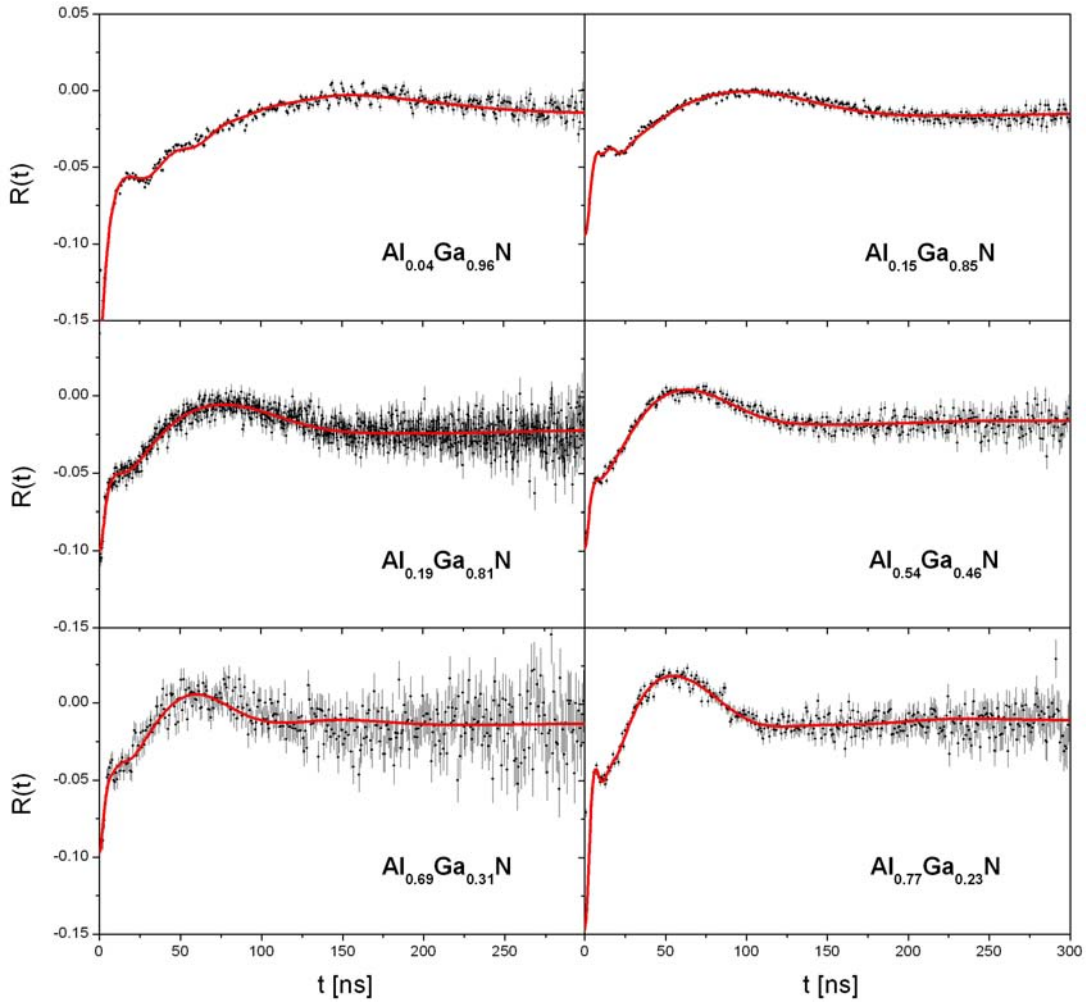

Figure C.1: *PAC-spectroscopy of tempered $Al_xGa_{1-x}N$ samples ($T_A = 1223\,\mathrm{K}$) depending on the AlN-content.*

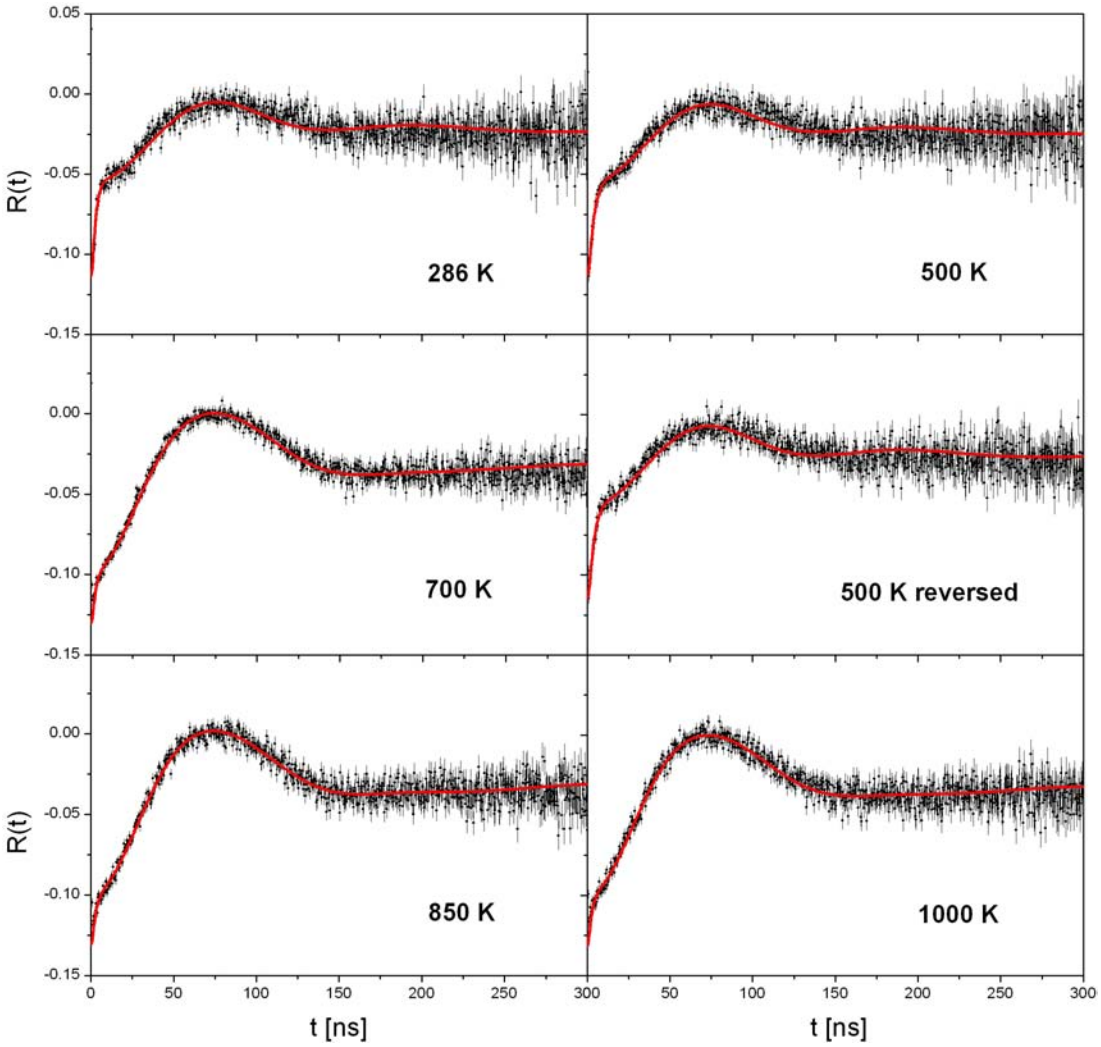

Figure C.2: *Temperature dependence PAC-spectroscopy of* ^{111}In *in* $Al_{0.19}Ga_{0.81}N$

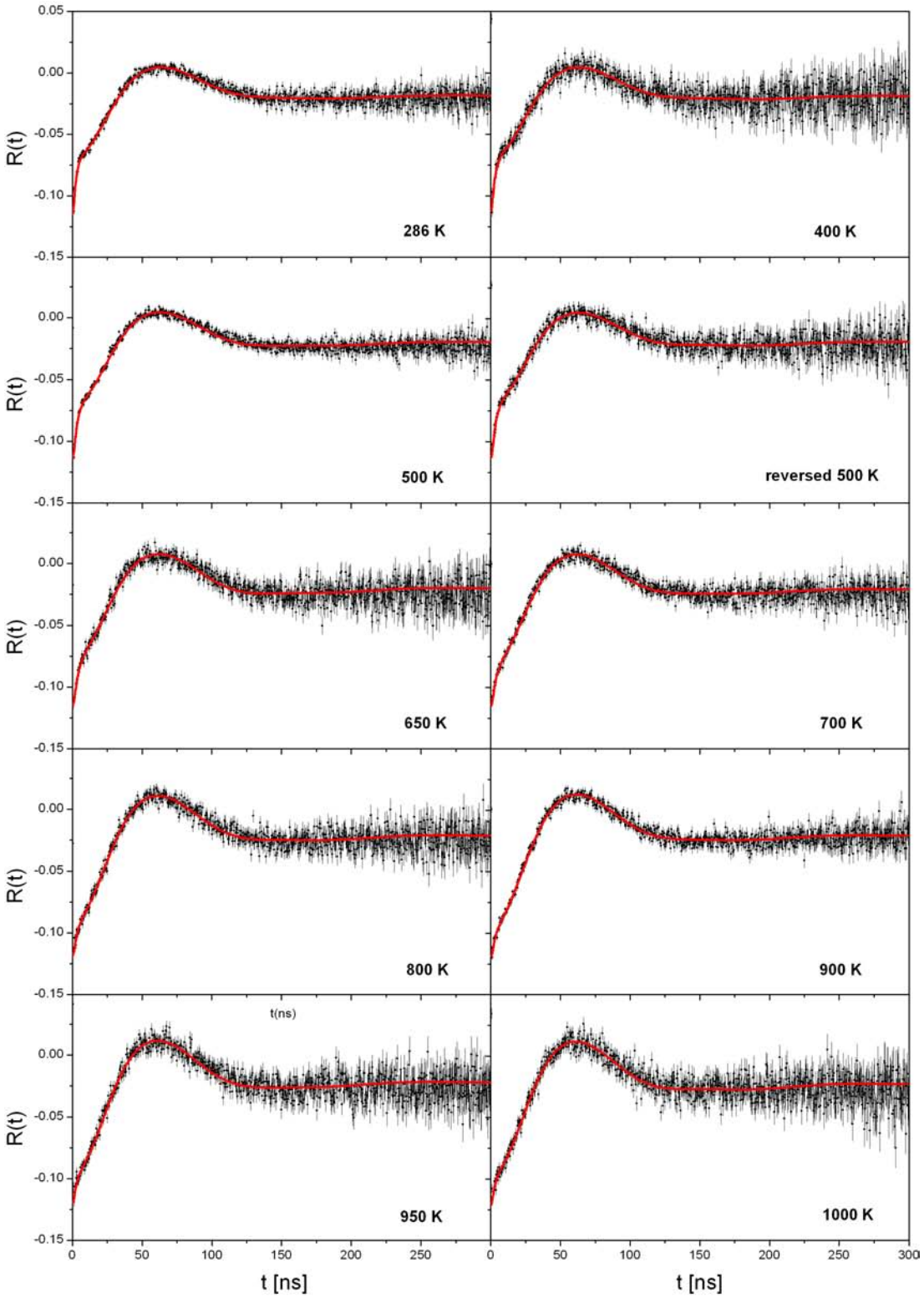

Figure C.3: *Temperature dependence PAC-spectroscopy of* ^{111}In *in* $Al_{0.55}Ga_{0.46}N$

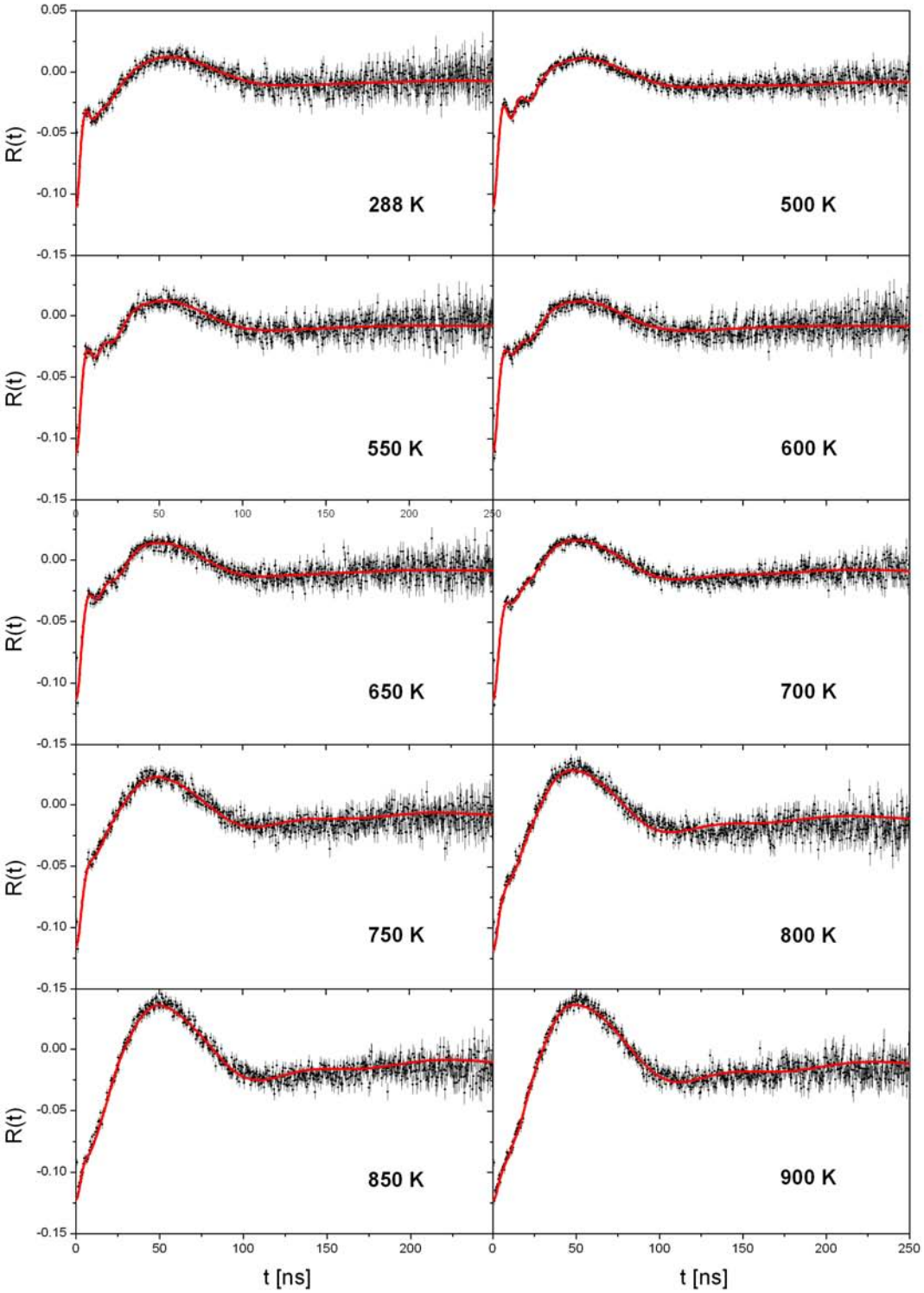

Figure C.4: *Temperature dependence PAC-spectroscopy of* ^{111}In *in* $Al_{0.77}Ga_{0.23}N$

.

Bibliography

[ALV08] E. Alves, J.P. Araújo, M. Barbosa, J.G.Correia, K. Johnston, P. Keßler, A.L. Lopes, K. Lorenz, S. Magalhães, J.G. Marques, J. Niederhausen, R. Vianden, *The role of In in III-nitride ternary semiconductors*, CERN-INTC-2008-038. INTC-P-251, (2008)

[ARE80] A.R. Arenda, C. Hohenemser, F. Pleiter, H. de Waard, L. Chow, R.M. Suter, Data Reduction Methodology for Perturbed Angular Correlation Experiments, *Hyp. Int. 8*: 191-213 (1980)

[ARE10] M. Arenz, *Aufbau und Test eines Hochtemperaturmessofens für γ-γ-Winkelkorrelationsmessungen*, Diploma Thesis, University of Bonn (2010)

[ARE] M. Arenz, University of Bonn, not published (2010)

[BAR92] N.P. Barradas, *NNFIT the PAC MANual*, Lissabon (1992)

[BEZ98] E. Bezakova, *Implantation Damage in Materials Studied by Hyperfine Interactions*, PhD thesis, Australian National University (1998)

[BH80] J.P. Biersack, L.G. Haggmark, A Monte Carlo Computer Program for the Transport of Energetic Ions in Amorphous Targets, *Nuclear Instruments and Methods 174*: 257-269 (1980)

[DBR03] Z. Dridi, B. Bouhafs, P. Ruterana, First-Principles Calculation of Structural and Electronic Properties of Wurtzite $Al_xGa_{1-x}N$, $In_xGa_{1-x}N$, and $In_xAl_{1-x}N$ Random Alloys, *physica status solidi (c) 0*: 315-319 (2003)

[DSB05] R. DOGRA, S. K. SHRESTHA, A. P. BYRNE, M. C. RIDGWAY, A. V. J. EDGE , R. VIANDEN, J. PENNER, H. TIMMERS, Evidence for atomic scale disorder in indium nitride from perturbed angular correlation spectroscopy, *J. Phys.: Condens. Matter 17*: 6037-6046 (2005)

[FS65] H. Frauenfelder and R.M. Steffen, *Alpha-, Beta- and Gamma-Ray Spectroscopy*,ed. K. Siegbahn, chapter XIX. North-Holland, Amsterdam (1965)

[GLV09] T. Geruschke, K. Lorenz, R, Vianden, Alloy and lattice disorder in HF implanted $Al_xGa_{1-x}N$ ($0 \leq x \leq 1$), *Physica B: Condensed Matter 404*: 4882-4885 (2009)

[IAG08] E. Iliopoulos, A. Adikimenakis, C. Giesen, M. Heuken, A. Georgakilas, Energy band gap bowing of InAlN alloys studied by spectroscopic ellipsometry, *App. Phy. Lett. 92*: 191907 (2008)

[IOFFE] Ioffe Physico-Technical Institute: *New Semiconductor Materials. Charachteristics and Properties*, Electronic archive, http://www.ioffe.rssi.ru/SVA/NSM/

[KEI01] M. Keiser, *Aluminiumnitrid-Schutzschichten auf Galliumnitrid - Herstellung und Charakterisierung*, Diploma Thesis, University of Bonn (2001)

[KES08] P. Keßler, *Implantationsschäden in Polaren und Unpolaren ZnO Einkristallen*, Diploma Thesis, University of Bonn (2008)

[LOR02] K. Lorenz, *Implantationsstudien an Gruppe-III-Nitriden*, Dissertation, University of Bonn (2002)

[LRV02] K. Lorenz, F. Ruske, R. Vianden, Reversible changes in the lattice site structure for In implanted into GaN, *Appl. Phys. Lett. 80*: 4531 (2002)

[LEE99] S. R. Lee, A. F. Wright, M. H. Crawford, G. A. Petersen, J. Han, R. M. Biefeld, The band-gap bowing of $Al_xGa_{1-x}N$ alloys, *Appl. Phys. Lett. 74*: 3344 (1999)

[MHP] L. Malikova, Y. S. Huang, F. H. Pollak, Z. C. Feng, M. Schurman, R. A. Stall, Temperature dependence of the energies and broadening parameters of the excitonic interband transitions in $Ga_{0.95}Al_{0.05}N$, *Solid State Commun. 103*: 273 (1997)

[MAR90] G. Marx, *Aufbau und Test einer RTA - Kurzzeit-Temper-Anlage*, Diploma Thesis, University of Bonn (1990)

[MOR99] H. Morkoç, *Nitride Semicondoctors and Devices*,Springer Berlin Heidelberg (1999)

[NÉD07] R. Nédélec, *Seltene Erden in GaN und ZnO untersucht mit der PAC-Methode*, University of Bonn, Diss. (2007)

[NIE09] J. Niederhausen, *Temperaturverhalten eines Indium-Defekt-Komplexs in Aluminiumnitrid*, Diploma Thesis, University of Bonn (2009)

[PEN07] J. Penner, *Lokale Gitterumgebung von Indium in GaN, AlN und InN*, University of Bonn, Diss. (2007)

[RUS01] F. Ruske, *Indiumimplantation in Galliumnitrid untersucht mit der γ-γ-Winkelkorrelationsmethode*, University of Bonn, Diploma Thesis (2001)

[SCH07] J. Schmitz, *PAC-Untersuchungen an Gruppe-III-Nitridhalbleitern mit der Sonde ^{111}In*, Diploma Thesis, University of Bonn (2007)

[SR93] M. Schulze-Rojahn, *Aufbau und Test eines PAC-Messofens und TDPAC-Messungen am System ^{111}In in $AgGaS_2$*.. Diploma Thesis, University of Bonn (1993)

[STE07] M. Steffens, *Hyperfeinwechselwirkung in dünnen Schichten des Gate-Dielektrikums HfO_2*, Diloma Thesis, University of Bonn (2007)

[SW92] G. Schatz and A. Weidinger., *Nuclear Condensed Matter Physics*, John Wiley and Son, New York (1992)

[UNB98] M. Uhrmacher, M. Neubauer,W. Bolse, L. Ziegeler, K. P. Lieb, Preparation of ion-implanted and sub-monolayer ^{111}In-tracer layers for perturbed angular correlation analysis, *Nuclear Instruments and Methods in Physics Research 139*: 306-312 (1998)

[VV10] R. Valentini, R. Vianden, PAC studies with LSO scintillation crystals, *Nuclear Instruments and Methods in Physics Research Section A* article in press (2010)

[WEG85] D. Wegner, Calculated Perturbed Angular Correlation for ^{111}In Doped Cubic Single Crystals, *Hyp. Int. 23*: 179-210 (1985)

[WEI96] S.-H. Wei, A. Zunger, Valance band splitings and band offsets of AlN, GaN and InN, *App. Phy. Lett. 69*: 2719-2721 (1996)

[WOL99] T. Wang, Y. Ohno, M. Lachab, D. Nakagawa, T. Shirahama, S. Sakai, H. Ohno, Electron mobility exceeding $10^4 \frac{\mathrm{cm}^2}{\mathrm{Vs}}$ in an AlGaN-GaN heterostrusture grown on a sapphire substrate, *App. Phy. Lett. 74*: 3531-3533 (1999)

Acknowledgment

At the first place I express my gratitude to Herr Priv. Doz. Dr. Reiner Vianden for his excellent supervision. Without his support and patience, studying this work was not possible.

I am very thankful to Herr Prof. Dr. K.-T. Brinkmann to accept the correction of this work.

I wish to say my special thanks to the whole Arbeitsgruppe for all the nice time we had together. Special thanks to my dear friend Marius and his family that were always beside me.

List of Figures